

## The many facets of molecular orientation in organic optoelectronics

Alexander Hofmann, Markus Schmid, Wolfgang Brütting

### Angaben zur Veröffentlichung / Publication details:

Hofmann, Alexander, Markus Schmid, and Wolfgang Brütting. 2021. "The many facets of molecular orientation in organic optoelectronics." *Advanced Optical Materials* 9 (21): 2101004. <https://doi.org/10.1002/adom.202101004>.

# The Many Facets of Molecular Orientation in Organic Optoelectronics

Alexander Hofmann, Markus Schmid, and Wolfgang Brütting\*

Over the years, organic optoelectronics have evolved into a mature technology with a wide range of applications. Their building blocks, namely organic semiconductors, are distinctly different from their inorganic counterparts due to orientational degrees of freedom that offer unique possibilities for tailoring their properties in thin-film structures. In this article, the many facets that molecular orientation has for fundamental aspects, like film growth as well as optical and electrical behavior, are reviewed and the implications of molecular orientation for device application are discussed.

## 1. Introduction

Over the last two decades, organic optoelectronics have evolved to a very successful technology for information display, for example, in smartphones or television screens, and beyond. These fascinating applications are based on unique properties of organic semiconductors in comparison to their inorganic counterparts, that is, elemental semiconductors, like Si, or compound materials, like GaAs—just to name two of the most prominent representatives of a larger family. Organic semiconductors allow large-area film deposition by low-cost processes, like printing or low-temperature vapor deposition, and due to their (mostly) non-crystalline nature they are compatible with a broad variety of different substrates, including flexible or bendable ones and (almost) arbitrary shapes.<sup>[1,2]</sup>

Another unique selling point are their orientational degrees of freedom which distinguish them from most of their inorganic counterparts. In contrast to elemental semiconductors, the building blocks of organic molecular solids are—as the name already says—molecules. They have internal degrees of freedom, that is, intramolecular vibrations in addition to intermolecular ones that correspond to phonons in crystalline solid, as well as orientational degrees of freedom, because with very few exceptions, like the fullerene C<sub>60</sub>,  $\pi$ -conjugated organic molecules have more or less anisotropic shapes.<sup>[3]</sup> These naturally lead to anisotropic electronic properties on the scale of the

individual molecules. However, if one can control molecular orientation on macroscopic length scales, for example, during the thin-film deposition process, this feature can be exploited to the benefit of optoelectronic device performance. Examples are improved charge carrier mobility in organic thin-film transistors along the conducting transport channel for vertically aligned molecules,<sup>[4]</sup> as well as higher light absorption in organic solar cells or improved light outcoupling in organic light-emitting diodes, if the  $\pi$ -conjugated

system of molecules or polymers is aligned preferentially in the film plane.<sup>[5–7]</sup>

Of course, such anisotropies have already been observed in organic molecular crystals that were investigated from the 1960s on.<sup>[8]</sup> An impressive example of birefringence—in the literal sense—in an anthracene single crystal is shown in **Figure 1**. However, even in the technically relevant thin films that are used nowadays, surprisingly high degrees of orientational order of the molecules can be found, even though the films are (in most cases) non-crystalline, that is, they do not exhibit long-range positional ordering. Note, that there are many semi-crystalline polymers or molecules growing as polycrystalline thin films where such order is observed. These are, however, not in the focus of this review, but rather the class of disordered (“glassy”) molecular solids.

As prerequisite for macroscopically observable optoelectronic anisotropy of a material, its molecular constituents must have non-centrosymmetric microscopic properties. As an example, **Figure 2** shows a hypothetical thin-film device stack consisting of three organic layers, like it is typically found in an organic light-emitting diode (OLED). The top-most layer is taken to be optically anisotropic, that is, it shows birefringence, the layer in the middle has improved light outcoupling due to preferential alignment of the light-emitting dipoles, while the layer at the bottom is assumed to exhibit a macroscopic dielectric polarization because of partially aligned polar molecules. The three subfigures illustrate how the macroscopic phenomena are related to microscopic molecular properties, which are the polarizability tensor, the optical transition dipole moment (TDM) or the permanent electrical dipole moment (PDM) of the constituent molecules. Also indicated are the order parameters that are typically used to quantify the degree of anisotropy, specifically the difference between the in-plane and out-of-plane components of the refractive index, the second moment of the angular distribution of TDMs with respect to the film normal and the interfacial polarization resulting from PDM alignment.

All of them are known to occur in specific materials or under certain preparation conditions, but their active control and

A. Hofmann, M. Schmid, W. Brütting  
Universität Augsburg, Institut für Physik  
86159 Augsburg, Germany  
E-mail: wolfgang.bruetting@physik.uni-augsburg.de

 The ORCID identification number(s) for the author(s) of this article can be found under <https://doi.org/10.1002/adom.202101004>.

© 2021 The Authors. Advanced Optical Materials published by Wiley-VCH GmbH. This is an open access article under the terms of the Creative Commons Attribution License, which permits use, distribution and reproduction in any medium, provided the original work is properly cited.

DOI: 10.1002/adom.202101004

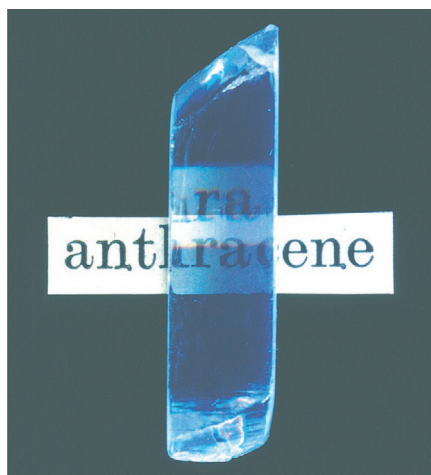


**Figure 1.** Example for birefringence in organic semiconductors: Bridgman-grown anthracene single crystal. The crystal is about 2 cm long and has a thickness of 1 cm. The  $c'$  direction of the crystal is along the direction of sight in the picture. (Color image reproduced with permission.<sup>[3]</sup> Copyright 2006, Wiley-VCH. The crystal was originally grown by N. Karl and a low-resolution image was published elsewhere. Adapted with permission.<sup>[9]</sup> Copyright 1989, Taylor & Francis).

exploitation in devices has only recently become a major topic in organic optoelectronics.<sup>[10–12]</sup> Moreover, as different (and sometimes competing) effects can even occur in one and the same type of device application, their underlying principles and design rules need to be well understood.

In this article, we review the current understanding of this emerging field of organic optoelectronics and discuss recent developments as well as some open issues.

## 2. Materials and Phenomena

Historically speaking, molecular orientation has been an important issue over the last 2 decades and researchers have always tried to use it as a handle to control certain device features.<sup>[13]</sup> Thus, there is also a hierarchy of complexity associated with molecular orientation. First, neat films consisting of a single molecular species were used, for example, in polymer light-emitting diodes or organic field-effect transistors. It was observed that shear forces during solution processing of long-chain polymers, sometimes in combination with surface treatment of substrates, can lead to orientation with the polymer backbone being preferentially aligned in the film plane.<sup>[5,14,15]</sup> For vapor-deposited molecular materials, the tendency for upright standing molecules was realized to be beneficial in OFETs, for example made from pentacene.<sup>[16,17]</sup> Such systems were typically grown at high temperature on inert or weakly interacting substrates, which resulted in highly crystalline thin films.<sup>[18]</sup>

Proceeding further, interface electronic structure between different neat materials was realized to depend critically on the mutual alignment of molecules in adjacent layers. Specifically, it was found that device-relevant energies of molecular frontier orbitals that determine ionization potential and electron affinity can vary as much as almost 1 eV, depending on the orientation

of molecules at a heterointerface.<sup>[19]</sup> This, obviously, has important consequences for charge carrier injection from electrodes or interfacial recombination as well as device relevant parameters like the open-circuit voltage of solar cells.<sup>[20–23]</sup>

However, not only neat layers of a single component can exhibit anisotropic behavior, but also mixtures or blends that are technically more relevant, for example, in organic photovoltaics.<sup>[24]</sup> In that context, the formation of co-crystals (or co-crystalline thin films) from structurally similar but electronically disparate materials, such as two molecular species where one is considered to act as electron donor and the other as electron acceptor, offers the unique possibility to study anisotropic charge-transfer (CT) interactions between them.<sup>[25]</sup> Examples are ground-state as well as excited-state CT complexes used for conductivity doping, photodiodes, and solar cells as well as carrier multiplication processes, such as singlet fission.<sup>[26–28]</sup>

More recently, even non-crystalline (“glassy”) molecular solids have been found to exhibit pronounced anisotropy of their optoelectronic properties and the controlled fabrication of such systems has become an active topic in glass physics (vide infra).<sup>[29]</sup> However, the most remarkable and unexpected aspect is probably the fact that even diluted guest–host systems, that is, molecular mixtures far from the equimolar ratio typically found in the above-mentioned co-crystals or blends, can have strongly anisotropic properties owing to preferential orientation of optical or electrical dipole moments of the guest molecules in an otherwise isotropic matrix. Prominent examples are dye-doped OLEDs with predominant horizontal emitter orientation for improved light outcoupling<sup>[11]</sup> or polar transport layers showing a macroscopic dielectric polarization.<sup>[30]</sup>

Before going into the details of how to prepare and characterize such anisotropic molecular layers as well as their relevance for devices, we will briefly introduce three main aspects in the context of organic optoelectronics, as schematically indicated in Figure 2.

- *Optical anisotropy* is a well-known feature of certain organic films (no matter if they are composed of molecular units or polymers), in particular if their building blocks have highly anisotropic molecular polarizability  $\alpha$  (see Figure 2c). In general,  $\alpha$  is a tensor that reflects how deformable the electron cloud of a molecule is along different axes. For organic semiconductors, the direction (or plane) of largest extent of  $\pi$ -conjugation is typically found to have the highest  $\alpha$ -component, whereas it is smallest perpendicular to that plane. Using, for example, the Clausius–Mossotti relation  $\alpha$  can be related to a macroscopic film property, namely the optical refractive index  $n$ :<sup>[31]</sup>

$$n \approx \sqrt{\frac{N\alpha}{\epsilon_0} + 1}, \quad (1)$$

with  $N$  being the number of molecules per unit volume and  $\epsilon_0$  the permittivity of vacuum. Typically, the preparation conditions used for organic semiconductor devices lead to isotropic refractive indices of films, if there is no preferential alignment of molecules. However, some degree of birefringence, that is, uniaxial alignment with the out-of-plane component  $n_e$  (the extra-ordinary refractive index)

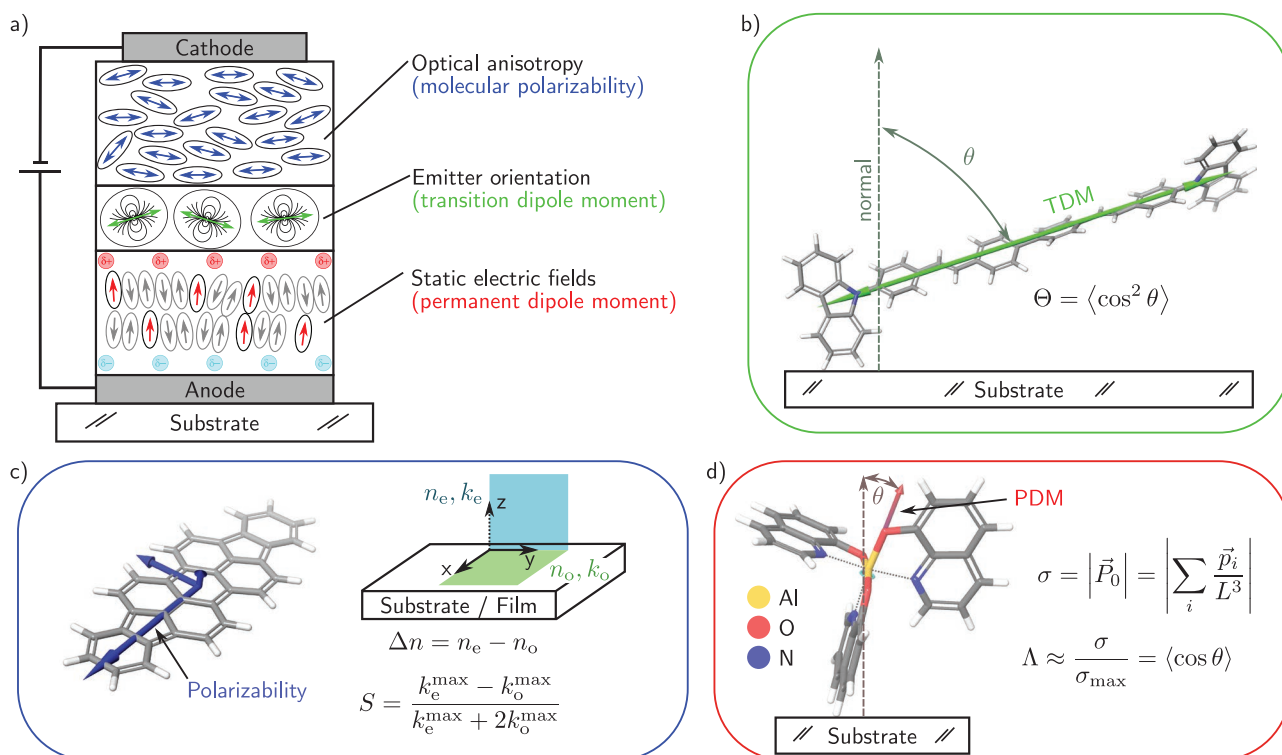


**Figure 2.** a) Exemplary device stack of an organic light emitting diode comprising molecules with different features of orientation. The basic physical phenomena and the corresponding order parameters are indicated for emitter orientation through transition dipole moment (TDM) alignment, optical anisotropy or birefringence, and dielectric polarization due to aligned permanent dipole moments (PDM) in the boxes (b) to (d), respectively.

being slightly different from the ordinary (in-plane) component  $n_o$  is also not uncommon. Depending on the sign,  $\Delta n := n_e - n_o$  indicates whether molecules are preferentially lying down on a substrate (“negative birefringence”) or whether they are standing up (“positive birefringence”) if their shape is rod- or disc-like.<sup>[10]</sup> A prominent example is DIP (shown in Figure 2c) where both scenarios have been observed.<sup>[32]</sup> The case that all three components of the refractive index are different—the so-called biaxial case—is found in molecular crystals, like the one shown in Figure 1. Typically, however, thin films of molecular materials are isotropic within the film plane and may exhibit certain anisotropy only in the out-of-plane direction with  $|\Delta n|$  of not more than 0.2. Exceptions from that rule are, for example, stretched polymer films or layers deposited under mechanical shear flow. In the context of optoelectronic devices, birefringence is relevant because it influences light propagation in stratified layered media.<sup>[33]</sup> For example, it has been demonstrated by simulation and verified experimentally that negative birefringence of the so-called electron transport layer in an OLED that is, the layer next to the metallic cathode (see Figure 2a), enhances light outcoupling by a few percent.<sup>[34,35]</sup> The reason is that the coupling of light emission to lossy waves, most importantly to surface plasmon polaritons, is predominantly transverse magnetic and can be reduced if the respective component of the refractive index in the organic layer(s) is smaller.

- However, most important for the efficiency of OLEDs is the feature that certain *emitter* molecules can be *aligned horizontally*, that is, with their optical transition dipole moment lying predominantly in the film plane.<sup>[11]</sup> This can be understood in a semiclassical picture of the radiation pattern of a dipole antenna, which is strongest in the direction perpendicular to the axis along which the charges forming the dipole oscillate.<sup>[36,37]</sup> The underlying molecular property is the quantum mechanical transition dipole moment (TDM) between the involved electronic ground and excited states. The TDM vector, which is usually obtained from time-dependent density functional theory (TD-DFT) calculations, has a well-defined direction relative to the molecular backbone that is related to the distribution of the involved molecular orbitals and is, thus, linked to the alignment of the molecule itself. For the example shown in Figure 2b, the TDM vector is parallel to the long axis of the rod-like BSB-Cz molecule.<sup>[10]</sup> Note that depending on the type of emitter material (fluorescence, phosphorescence, or thermally activated delayed fluorescence) a molecule may have several TDM vectors with different lengths, that is, oscillator strengths, and directions that need to be considered. If  $\theta$  is the angle between the TDM vector and the film normal, the orientation parameter is given by the second moment of the TDM distribution around this axis:<sup>[11]</sup>

$$\Theta = \langle \cos^2 \theta \rangle \quad (2)$$

Also common is the use of an order parameter  $S$  that is defined in a slightly different manner and can be determined from the anisotropy found in the extinction coefficients of birefringent materials, that is, from the inverse of the light emission process,<sup>[10]</sup> see Figure 2c):

$$S = \frac{k_e^{\max} - k_o^{\max}}{k_e^{\max} + 2k_o^{\max}} \quad (3)$$

- The third orientation parameter, which will be discussed in this review, is the *permanent dipole moment* (PDM) and its alignment—if there is any (see Figure 2d). Of course, highly symmetric molecules will not have a PDM, and are therefore said to be non-polar, because the centers of negative and positive charge distributions coincide. However, if this is not the case, for example, due to asymmetries in the chemical structure of the molecule or non-planarity of molecules that look symmetric in a simple 2D drawing of their structure, molecules will have a non-vanishing PDM and, thus, be polar. Note that even if a molecule does not exhibit a sizeable PDM in the ground state, it can do so in the excited state, and directions of the respective PDM vectors can be different as well. This is particularly pronounced if the excited state has charge-transfer character, as it is the case for thermally activated delayed fluorescence (TADF) emitters, and can induce remarkable photophysical effects that are the subject of dedicated studies<sup>[38,39]</sup> but will not be discussed here. The focus of this review are polar molecules that show a non-vanishing net alignment of their PDMs in thin films, so-called spontaneous orientation polarization (SOP).<sup>[30]</sup> As indicated in Figure 2d, this leads to a macroscopic dielectric polarization  $P_0$  which is related to the presence of interfacial charge densities  $\sigma$  of opposite sign at the interfaces to neighboring layers, if those are non-polar, and is described by an order parameter

$$\Lambda = \langle \cos \theta \rangle \quad (4)$$

where, in this case,  $\theta$  is the polar angle between the PDM vector and the surface normal. If the free surface of such a film is considered, it will exhibit a non-zero surface potential proportional to the thickness of the layer, which is often called the “giant surface potential” (GSP). A prototypical example is the  $\text{Alq}_3$  molecule, where this phenomenon has been reported already 20 years ago.<sup>[40,41]</sup>

### 3. Measuring Molecular Orientation

Measuring molecular orientation of organic semiconductors will always rely on a specific phenomenon or a “probe” so to speak, which after measurement can be traced back to the orientation of the molecule. Unlike measurements on single crystals with, for example, X-ray diffraction, in glassy or amorphous systems the majority of molecules will most probably not show one specific orientation, but rather a broad range of possible angles around the substrate normal. The obtained “orientation” of molecules in the film is thus, in most cases, only a mean value of a specific distribution of orientational angles.

Also, different techniques probe different properties of the molecules, whose link to each other are not a priori known and might also differ significantly in the degree of alignment. For example,  $\text{Alq}_3$  can show a distinct orientation of its permanent dipole moment, but no alignment of the transition dipoles has been detected so far.<sup>[42]</sup> In this section, we will present an overview of different methods to determine molecular orientation in organic thin films. A summary is also given in Table 1. In the end, we show how computer simulations can help to combine individual quantities to a comprehensive picture of molecular orientation. Note that there are further techniques that will not be covered here, for example non-linear optical measurements<sup>[43]</sup> or nuclear magnetic resonance.<sup>[44]</sup>

#### 3.1. Optical Orientation: The Transition Dipole Moment

As the orientation of the transition dipole moments in OLEDs plays a crucial role for their efficiency, some very robust techniques exist to assess their alignment in a film. First of all, for OLEDs, the emissive TDM is the one to optimize, the absorbing TDMs do not need to be oriented the same way. As pointed out in Section 2, to describe the emissive TDM orientation, the factor  $\Theta$  has been introduced, which is given by<sup>[11]</sup>

$$\Theta = \frac{\sum_i p_{z,i}^2}{\sum_i |\vec{p}_i|^2} = \frac{\sum_i (|\vec{p}_i| \cos(\theta_i))^2}{\sum_i |\vec{p}_i|^2} = \langle \cos^2 \theta \rangle \quad (5)$$

where  $\vec{p}$  is the molecule’s TDM vector and the sum goes over all molecules in the film. The latter equality is, of course, only valid if all molecules have the same magnitude of their TDM.  $\Theta$  refers to the portion of energy emitted by transition dipoles oriented perpendicular to the film surface and should be close to zero for a high light outcoupling efficiency due to horizontally aligned dipoles. Isotropic orientation will yield  $\Theta \approx 0.33$  and a completely vertical emitter orientation leads to  $\Theta = 1$ . If the system is being described with one single “effective” TDM angle, it is linked to the orientation factor with  $\langle \theta \rangle = \arccos(\sqrt{\Theta})$ .

For molecules with different conformers in the solid film or phosphorescent emitter complexes with more than one emissive TDM per molecule, Equation (5) can be extended to read<sup>[51]</sup>

$$\Theta = \frac{\sum_i \Phi(\theta_i) \sum_j \frac{k_{r,j}}{k_{\text{tot}}} p_z^2(i, j)}{\sum_i \Phi(\theta_i) \sum_j \frac{k_{r,j}}{k_{\text{tot}}} |\vec{p}(i, j)|^2} \quad (6)$$

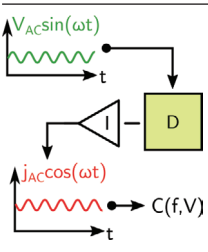
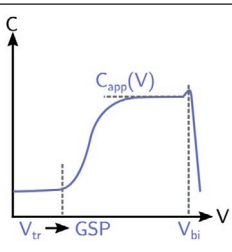
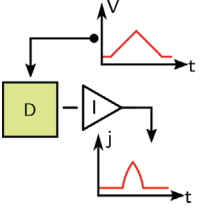
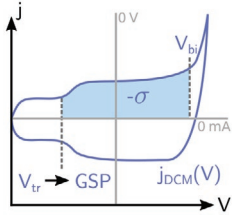
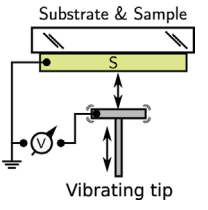
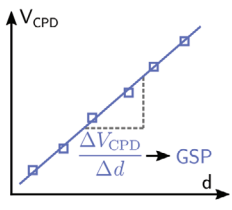
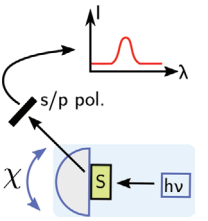
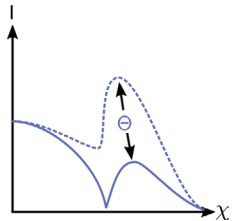
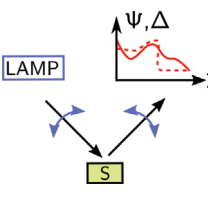
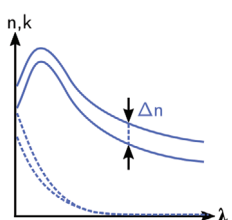
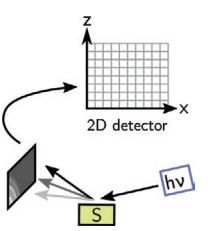
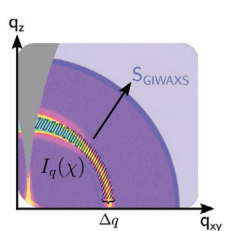
Here, each molecule  $i$  and each emissive TDM  $j$  on the molecule are considered individually. The distribution function  $\Phi(\theta_i)$  specifies the probability of a specific molecular orientation in the film and  $k_r$  the radiative rates of the individual TDMs in relation to the total excited state decay rate  $k_{\text{tot}}$ .

##### 3.1.1. Angular Dependent Photoluminescence

For any measurement of the emitter orientation using an optical approach, it needs to be traced back to the radiation



**Table 1.** Overview on different methods to determine molecular orientation in organic thin films. In the left-most column, a sketch of the measurement method is given, followed by a brief description of the method, more details are given in the text. Additionally, a sketch of the data indicating the basic principle of parameter-extraction from the measurement is drawn. The sample (S), usually a thin film, or device (D), typically a diode, are highlighted in green. For references, see the right-most column.

Sketch	Name, description	Measurement	References
	<b>Impedance Spectroscopy (IS)</b> C(V) measurement at constant frequency. Hole accumulation changes the apparent device capacitance; the transition voltage $V_{tr}$ can be traced back to the GSP.		[45]
	<b>Displacement Current Measurements (DCM)</b> Fast (transient) $j(V)$ measurement aiming for the capacitive response of the device. Charge accumulation leads to a step, which is traced back to the GSP. Integration between $V_{tr}$ and $V_{bi}$ yields the accumulated charge. Differences in the amount of injected (forward sweep) and extracted charge (backward sweep) indicates charge trapping in the device.		[46]
	<b>Kelvin Probe (KP)</b> Direct observation of the surface potential of the thin film in dependence of its thickness. The slope of potential versus thickness corresponds to the GSP.		[41]
	<b>Angular dependant PL (ADPL)</b> Measured (spectral) intensity of s- and p-polarized light emission through a macroextractor in angular dependence. The orientation of the emissive TDM is gained by fitting simulation data.		[47,48]
	<b>Variable angle spectroscopic ellipsometry (VASE)</b> Angular dependent (spectral) transmission/reflection. Birefringence is visible in the (fitted) data for $\Delta n = n_e - n_o$ or the order parameter $S$ from the maxima of the (fitted) extinction coefficient.		[10,49]
	<b>Grazing incidence wide-angle X-Ray scattering (GIWAXS)</b> X-Ray scattering at very low incident angles. The scattering pattern provides information about in-plane and out-of-plane order of organic molecules.		[50]

pattern of the emission. In angular dependent photoluminescence (ADPL), the excitation light is directed perpendicular to the film surface and the photoluminescence spectrum recorded in different angles behind a half-sphere macroextractor, ideally

using a polarizer (for a more in-depth description of the setup see for example, ref. [47], a small sketch is presented in Table 1). The total emitted intensity of a single dipole can be described with one component parallel and one perpendicular to the

substrate,  $p_{\parallel}$  and  $p_{\perp}$ , respectively. Furthermore, the parallel emission can be separated into  $s$ - and  $p$ -polarized electromagnetic waves, whereas the perpendicular component will only be  $p$ -polarized. Then the observed radiation pattern is given as<sup>[52]</sup>

$$I(\chi, \vec{r}, \lambda, \theta) = \cos^2 \theta (I_{\perp, p}(\chi, \vec{r}, \lambda)) + \sin^2 \theta (I_{\parallel, s}(\chi, \vec{r}, \lambda) + I_{\parallel, p}(\chi, \vec{r}, \lambda)) \quad (7)$$

In this expression,  $\theta$  again is the orientation of the individual dipole and  $\vec{r}$  its position in the emission layer. The radiation pattern is then dependent on the observation angle external to the layer stack  $\chi$ , as well as the wavelength  $\lambda$ . From Equation (7) follows, that the measured  $s$ -polarized spectra  $I_s(\lambda)$  thus only contain emission from dipoles parallel to the surface, where  $I_p(\lambda)$  consist of a superposition of horizontal and vertical contributions. The orientation factor  $\Theta$  is then defined as

$$\Theta = \frac{P(p_{\perp})}{P(p_{\parallel}) + P(p_{\perp})} \quad (8)$$

where  $P$  denotes the integrated emissive power. To disentangle those contributions and determine the orientation factor, computer simulations with suitable models are needed.<sup>[11,33,47,53]</sup> In short, the  $s$ -polarized measurement can be used to determine the thickness of the film first; then a fit of the relative contributions of horizontal and perpendicular components can be conducted against the  $p$ -polarized spectra to determine  $\Theta$ . As a rule of thumb, the integrated intensity of the  $p$ -polarized spectra at angles around  $\approx 50^\circ$ , above the critical angle of total reflection, shift to higher intensities relative to the  $0^\circ$  emission for more vertical orientation, see sketch in Table 1.

### 3.1.2. Angular Dependent Electroluminescence

In contrast to ADPL, angular dependent electroluminescence does not rely on external excitation, but instead measures the signal emitted from a complete OLED stack.<sup>[48,54]</sup> However, because the reflecting cathode layer creates a micro-cavity inside the OLED, the layer thicknesses have to be tailored to create a detuned cavity for horizontal dipoles.<sup>[11]</sup> An optimized OLED stack for maximized light output will otherwise trap most of the emission from perpendicular oriented dipoles,<sup>[48]</sup> which would falsify the result. If, however, the emitter-cathode distance can be optimized for constructive interference of perpendicular dipoles, fitting the measured angular dependent spectra not only yields the average dipole orientation, but also allows to draw conclusions on the spatial emission profile, that is, the emission zone, as well.<sup>[48,55,56]</sup>

#### 3.1.3. Fourier-Plane Imaging

An alternative to the angular scanning approach is 2D Fourier-plane imaging microscopy, also known as back-focal-plane imaging.<sup>[57,58]</sup> Instead of scanning the angle and detecting the intensity of emitted light at every point, the diffraction pattern of the sample's emission as obtained through a Fourier lens is recorded through a 2D camera. By fitting the

measured patterns with a suitable model, the technique allows for a very fast and highly sensitive detection of the average dipole orientation.

### 3.2. Electrical Orientation: The Permanent Dipole Moment

An asymmetric charge distribution on a molecule in the ground state will lead to the formation of a permanent dipole moment (PDM), equal to what is known from polar molecules like water.<sup>[30]</sup> For organics, the magnitude of the PDM is usually in the range of 1D to 10D. (Molecules with a PDM of significantly less than 1D would be considered as non-polar).

Spontaneous orientation polarization can lead to a non-isotropic distribution of the PDMs of individual molecules, which in turn creates a macroscopic polarization throughout the whole film.<sup>[41]</sup> All electric measurements available to assess the orientation of the PDM target the strength of the film polarization. If the magnitude of the dipole as well as its orientation with respect to the molecular axes is known, conclusions can be drawn on the orientation of the molecule itself.<sup>[51]</sup>

In total, the overall polarization  $\vec{P}_0$  of the film is given as<sup>[30]</sup>

$$\vec{P}_0 = \sum_i \frac{\vec{p}_i}{L^3} \quad (9)$$

Here,  $\vec{p}_i$  is the PDM vector of the molecule  $i$  with magnitude  $|\vec{p}_i| = p$  in the film of volume  $L^3$ . In electrical measurements, usually only the component of  $\vec{P}_0$  parallel to the surface normal is accessible. Considering this to be the “ $z$ ” direction, only the scalar  $p_z = \vec{p}_i \times \vec{z}$  needs to be considered. Then, let  $\theta$  be the angle of the PDM of a molecule in the film in respect to the surface normal. This leads to the simplified expression of the film polarization<sup>[30]</sup> with

$$P_0 = \frac{p \sum_i \cos \theta_i}{L^3} = p \Lambda N \quad (10)$$

where  $\Lambda = \langle \cos \theta \rangle$  corresponds to the average orientation of PDMs in the film and  $N$  is the number of polar molecules per unit volume. In order to draw conclusions on the molecular orientation, however, the non-linear contribution of the cosine has to be considered alongside with the distribution function  $\Phi(\theta)$  of molecules with a certain orientation in the film. As a result,

$$\Lambda = \frac{\sum_i \Phi(\theta_i) \cos \theta_i}{N L^3} \quad (11)$$

It is important to note, however, that the average orientation of PDMs  $\langle \cos \theta \rangle$  does not necessarily correspond to the most preferential orientation of molecules in the film. In order to assess molecular orientation though, the orientation of the PDM alone is hence not sufficient.<sup>[51]</sup> Furthermore, since  $\Lambda$  represents the first moment of the PDM orientation distribution, one has to be aware that antiparallel PDMs cancel out and may, thus, lead to  $\Lambda = 0$ , even though the molecules are highly aligned.

Macroscopically, the film polarization  $P_0$  corresponds to the interfacial charge density  $\sigma$  induced by the oriented dipoles at both film surfaces.<sup>[30]</sup> Also, the integral over all oriented dipoles through the thickness of the film reveals an electrical potential

at the surface. Assuming a constant polarization throughout the whole film, it can be expressed as

$$V_s = \frac{\sigma}{\epsilon \epsilon_0} d \quad (12)$$

where  $\epsilon$  is the dielectric constant of the film. This potential, or voltage to be more precise, has been earlier identified as the giant surface potential (GSP).<sup>[41]</sup> A link to the figure of merit  $\Lambda$  is possible, if the actual  $\sigma$  and a hypothetical maximum interface charge  $\sigma_{\max}$  assuming all dipoles would orient along the surface normal are set in relation to each other. From Equation (10),  $P_{\max} = \sigma_{\max} = pN$ . Or in turn, if  $\sigma = P_0$  is measured,

$$\Lambda \approx \frac{\sigma}{\sigma_{\max}} \quad (13)$$

Depending on the method, either the GSP slope or the interface charge is directly available, both are linked by the dielectric constant and thus also sometimes used synonym in literature. In the following, common methods to determine either of them shall be briefly explained.

### 3.2.1. Kelvin Probe

Among the first measurements, where SOP and the resulting GSP has been seen, is the Kelvin probe technique. It measures the contact potential difference  $V_{CPD}$  between a vibrating tip and the sample surface (see Table 1). In order to determine the polarization of the film, the surface potential is recorded with increasing thickness.<sup>[41]</sup> The change in contact potential difference over thickness then corresponds to the GSP slope, or the internal field

$$E_{GSP} = \frac{\Delta V_{CPD}}{\Delta d} = \frac{\sigma}{\epsilon \epsilon_0} \quad (14)$$

The GSP slope is usually given in units of mV nm<sup>-1</sup>, value-equivalent to MV m<sup>-1</sup>. Without SOP, the measured contact potential would still resemble interface bound effects including a possible interface dipole and band-bending in the organic film.<sup>[59]</sup> Although the effect of the GSP on the measured CPD is much larger for a strongly polar film, interface properties are still visible in measurements of sufficient thickness resolution<sup>[41]</sup> even between two organic layers.<sup>[46]</sup> Additionally, the Kelvin probe technique has no prerequisites on the direction of the GSP and allows to reliably determine positive or negative interface charges.<sup>[60–62]</sup> Considering possible variations in film growth for lower thicknesses, it is good practice to choose film thicknesses and the range of evaluation large enough to exclude interface effects from the measured GSP of the bulk material.

### 3.2.2. Impedance Spectroscopy

Impedance spectroscopy (IS) measures the electric response of the sample dependent on the frequency of an applied AC

voltage possibly including a DC offset. To determine the interfacial charge density of a polar layer, it needs to be incorporated into a two-layer device together with a suitable charge transport layer. This is the case for example in a simple NPB/Alq<sub>3</sub> OLED, the device structure where the technique was first used to determine interface charges in polar organic layers.<sup>[40,45]</sup> Here, NPB serves as hole transport layer, and Alq<sub>3</sub> is the polar ETL processed on top of NPB in the stack. To determine  $\sigma$ , a measurement of the total capacitance of the OLEDs is performed at a fixed frequency with the external DC bias swept from negative voltages to above the built-in voltage  $V_{bi}$ . Typically, a pronounced step in the apparent device capacitance  $C_{app}$  can be observed (see Table 1). At high negative bias, where the device can be considered to be in depletion as no charge carriers can be injected in either layer, the measured capacitance will read  $C_{app}^{-1} = C_{HTL}^{-1} + C_{ETL}^{-1}$  as the two layers are stacked on top of each other. When the bias increases, the field gradient induced by the GSP in the ETL allows hole injection into the HTL far below  $V_{bi}$ . This leads to a step in  $C_{app}$  starting at a transition voltage  $V_{tr}$  which will finally lead to enhanced apparent device capacitance because the HTL has already reached flat-band conditions although the ETL is still reversely biased. Thus, the measured capacitance only resembles the ETL or  $C_{app} \approx C_{ETL}$ .

The change in capacitance at the transition voltage  $V_{tr}$  thus relates to the onset of hole injection into the HTL, which is shifted to below  $V_{bi}$  because of SOP. When  $V_{bi}$  is known, the GSP slope can thus be expressed by

$$E_{GSP} = \frac{V_{bi} - V_{tr}}{d_{ETL}} = \frac{\sigma_{ETL}}{\epsilon_{ETL} \epsilon_0} \quad (15)$$

The positive charges accumulated at the interface will only be neutralized after injection of electrons starts above the turn on or built-in voltage  $V_{bi}$ , or extracted when a large negative bias is applied, see also the DCM method.

It is worth a note, that this technique will allow only those polar layers to be investigated, whose SOP causes a shift toward negative voltages in respect to  $V_{bi}$ . Otherwise, hole and electron injection cannot easily be disentangled.

### 3.2.3. Displacement Current

Displacement current measurements (DCM) target the same microscopic process and device structure like impedance spectroscopy, but use a different measurement approach. Instead of measuring the device capacitance directly, the current-voltage characteristic is recorded using a triangular voltage at a speed sufficiently below the transient response of the device.<sup>[46]</sup> The measured current is then dominated by the displacement current induced by the charging of the device capacitor:

$$j_{DCM}(V) = \frac{dV}{dt} C_{app} + j_{diode} \quad (16)$$

where  $dV/dt$  is the slope of the voltage ramp and  $j_{diode}$  the steady-state diode current. The latter is easily eliminated by ramping the voltage up and down and subtracting both contributions



(see Table 1). Just as it is the case for IS, hole accumulation leads to a change in the apparent capacitance  $C_{app}$  starting at  $V_{tr}$ , the calculation of the magnitude of  $\sigma$  then follows Equation (15).

In case of DCM, however, an alternative approach has been established to calculate the interfacial charge density. The integral of the measured current or capacitance  $C_{app}$ , calculated from Equation (16), between  $V_{tr}$  and the built-in voltage of the device will give the charge carrier density accumulated in the HTL, with

$$-\sigma = \int_{V_{tr}}^{V_{bi}} j_{DCM}(t) dt = \int_{V_{tr}}^{V_{bi}} C_{app}(V) dV \quad (17)$$

As accumulation occurs until the interface charges have been compensated by injected carriers,<sup>[45]</sup>  $\sigma$  corresponds to the interface charge density. Note, however, that the exact definition of the integration boundaries and  $V_{tr}$  is a little bit more subtle; for details see ref. [46].

Because both impedance spectroscopy and DCM target the same processes in the device, the same limitations apply accordingly. Compared to IS, DCM however also allows to determine injected and extracted carriers simultaneously. This additionally allows to investigate trapped charges in comparison to the interface charge effects.<sup>[46]</sup>

### 3.3. Optical Anisotropy – Ellipsometry

Ellipsometry is a well-established method giving insight into the thickness and, in this context more importantly, the optical constants ( $n$ ,  $k$ ) of thin films. The method relies on the fact that the polarization state of light changes when the electromagnetic wave is interacting with thin films. The sample is typically illuminated under oblique angles with a polychromatic lightsource with defined polarization state and the polarization change of the specular reflected radiation is analyzed in terms of the so-called ellipsometric angles  $\Psi$  and  $\Delta$  (see Table 1). In order to resolve an optical anisotropy of the out-of-plane component of the (complex) refractive index, the angle of incidence needs to be varied for one sample.<sup>[10,63]</sup> As a large set of wavelengths and multiple angles are analyzed, the term variable angle spectroscopic ellipsometry (VASE) is commonly used.<sup>[10,49,64]</sup> An in-plane anisotropy can be resolved by a rotation of the sample,<sup>[63]</sup> but this effect is not relevant in the context of amorphous thin films as discussed in Section 1.<sup>[10]</sup>

In order to extract information about the optical constants from the measured ellipsometric angles  $\Psi$  and  $\Delta$ , the measurement is fitted with a model for the dispersion relation satisfying the Kramers–Kronig consistency.<sup>[63]</sup> Depending on the spectral range of interest and the investigated material, different dispersion relations are commonly applied. Common models therefore are the Cauchy layer model<sup>[65,66]</sup> as well as the Lorentz,<sup>[63]</sup> Gaussian, and the Tauc–Lorentz oscillator models.<sup>[67]</sup> In most cases, a linear combination of different dispersion relations is used to fit the experimental results,<sup>[64,68]</sup> a more systematic overview is given in textbooks like ref. [69]. If an optical anisotropy resulting from predominant molecular alignment is observed, a single dispersion will not be able to reproduce the

$\Psi$  and  $\Delta$  values at multiple angles.<sup>[68]</sup> Instead, one dispersion for the in-plane component ( $n_o$ ,  $k_o$ ) and another one for the out-of-plane component ( $n_e$ ,  $k_e$ ) is required. Note that the fitting of the experimental data often requires a large number of free parameters. This can make the determination of the optical constants a time consuming and challenging task.<sup>[70]</sup>

The dielectric function of the film is closely related to the molecular properties in the film. Far off the resonance frequency of the oscillator, where no absorption is observed, the refractive index is dominated by the electronic polarizability  $\alpha$  of molecules in the VIS/NIR-region of the spectrum.<sup>[71]</sup> Thus the birefringence  $\Delta n$  defined as

$$\Delta n = n_e - n_o \quad (18)$$

is a measure of the molecular orientation with respect to the electronic polarizability tensor  $\alpha$ . Furthermore, the absorption of the film is closely related to the transition dipole moments of the molecules. Therefore, the parameter  $S$  is established to quantify the orientation of the absorbing dipole moments in the film

$$S = \frac{k_e^{\max} - k_o^{\max}}{k_e^{\max} + 2k_o^{\max}} = \frac{3\langle \cos^2 \theta \rangle - 1}{2} \quad (19)$$

where  $k_o/e^{\max}$  are the maxima of the ordinary/extraordinary extinction coefficient and  $\langle \cos^2 \theta \rangle$  describes the ensemble average of the angle  $\theta$  between the substrate normal and the transition dipole moment for absorption.<sup>[10,11]</sup> For molecules where the TDMs for light absorption and emission are basically identical, the  $S$  parameter is easily related to the emissive TDM orientation parameter  $\Theta$  via  $S = \frac{1}{2}(3\Theta - 1)$ .

Finally, we want to mention, that a similar order parameter can be calculated for the refractive index, in case the electronic polarizability tensor is axially symmetric (two equal eigenvalues  $\alpha_1$  and one other eigenvalue  $\alpha_2$ ):

$$S_n = \frac{3\langle \cos^2 \theta_n \rangle - 1}{2} = \left[ \frac{3(n_e^2 - 1)}{n_e^2 + 2} - \frac{3(n_o^2 - 1)}{n_o^2 + 2} \right] \times \frac{N\epsilon_0}{\alpha_1 - \alpha_2} \quad (20)$$

In this context,  $\theta_n$  describes the angle between the symmetry axis of the polarizability tensor and the substrate normal and  $N$  the number of molecules per unit volume.<sup>[72,73]</sup> To the best of our knowledge, this parameter is not frequently applied in order to quantify the orientation of organic semiconductors.

### 3.4. Structural Anisotropy – X-Ray Scattering

Besides electrical and optical experiments, X-ray or even neutron scattering can of course also be utilized to probe molecular orientation. The low scattering cross section of organic thin films, however, renders classical X-ray experiments difficult,<sup>[74]</sup> except for, for example, highly ordered, rod-shaped small molecules like the perylene derivative DIP.<sup>[18]</sup> In contrast, grazing incidence X-ray scattering (GIXS) has evolved to a versatile tool for organic thin-film characterization<sup>[74]</sup> and has also recently been applied to vapor deposited glasses.<sup>[42,50]</sup> To analyze struc-

tures in molecular length scales, a large angular range of the scattered beam has to be recorded by grazing incidence wide-angle X-ray scattering (GIWAXS). Its small-angle counterpart GISAXS, in contrast, allows to probe the mesoscopic domain morphology of a larger lateral area in the thin film.<sup>[74]</sup> Common to both methods, however, is the very small incident angle  $\alpha < 1^\circ$  with respect to the sample surface of the highly monochromatic (synchrotron) X-ray radiation. The scattered beam is recorded with a 2D detector to probe in-plane and out-of-plane scattering at once.<sup>[74]</sup>

By analyzing the recorded 2D image in reciprocal space, one axis of the GIWAXS image corresponds to the momentum transfer  $q_z$ , that is, out-of-plane, the other to the in-plane, combined  $q_{xy}$  component (see sketch in Table 1). A GIWAXS order parameter  $S_{\text{GIWAXS}}$  can then be derived from the average intensity distribution along the angle  $\chi$  in reciprocal space<sup>[50]</sup>

$$S_{\text{GIWAXS}} = \frac{1}{2} (3 \langle \cos^2 \chi \rangle - 1) \quad (21)$$

ranging from 1.0 for a sharp intensity peak along  $q_z$  to  $-0.5$  for a  $q_{xy}$  feature. In Equation (21),  $\langle \cos^2 \chi \rangle$  is defined by

$$\langle \cos^2 \chi \rangle = \frac{\int_{0^\circ}^{90^\circ} I_q(\chi) \cos^2 \chi \sin \chi d\chi}{\int_{0^\circ}^{90^\circ} I_q(\chi) \sin \chi d\chi} \quad (22)$$

where the integration is performed along an arc with constant  $q$  value ( $q = \sqrt{q_{xy}^2 + q_z^2}$ ) with finite width  $\Delta q$  in the reciprocal space map and  $\chi = 0^\circ$  is along the  $q_z$  direction (see Table 1). By choosing the position of integration in reciprocal space near the nearest-neighbor distance of the molecules,  $S_{\text{GIWAXS}} \approx 1$  indicates face-on molecular stacking or layering, where lower or negative values point toward edge-on orienta-

tion.<sup>[42,50]</sup> Although an in-depth discussion of the GIWAXS technique is beyond the scope of this review, it is worth noting that the order parameter  $S_{\text{GIWAXS}}$  was found to be in line with for example, the order parameter extracted from ellipsometry.<sup>[50]</sup> Also, GIWAXS measurements proved molecular layering in Alq<sub>3</sub> thin films grown at room temperature and showed increasingly isotropic orientation for higher substrate temperatures.<sup>[42]</sup>

### 3.5. Computer Simulation

In the previous sections, methods for measuring different molecular orientation order parameters were discussed. However, the interpretation of the experimental data requires detailed and reliable information about the magnitude and directions of PDM, TDMs, and polarizability on the molecular framework. Two examples to illustrate this are Ir complexes or Alq<sub>3</sub> (see Figure 3). For the former, Friedrich et al., showed that many of the complexes only exhibit a small optical orientation anisotropy  $\Theta$ , although a significant alignment of the dye molecules was present in their simulations.<sup>[75]</sup> They explained this behavior with the different directions of multiple TDM vectors responsible for the light emission. For Alq<sub>3</sub>, the macroscopic dielectric polarization of films has been studied intensively.<sup>[40,41,59]</sup> However, Alq<sub>3</sub> films are optically isotropic because the polarizability is equal in all spatial directions.

In general, assessing thin-film electronic properties and potential anisotropies thereof, requires a two step approach: i) calculation of the individual molecules and ii) simulating their arrangement and interactions in the solid film.<sup>[78]</sup> For single, isolated molecules TD-DFT is established in order to predict the molecular geometry as well as the previously mentioned quantities for the gas-phase structure. Moreover,

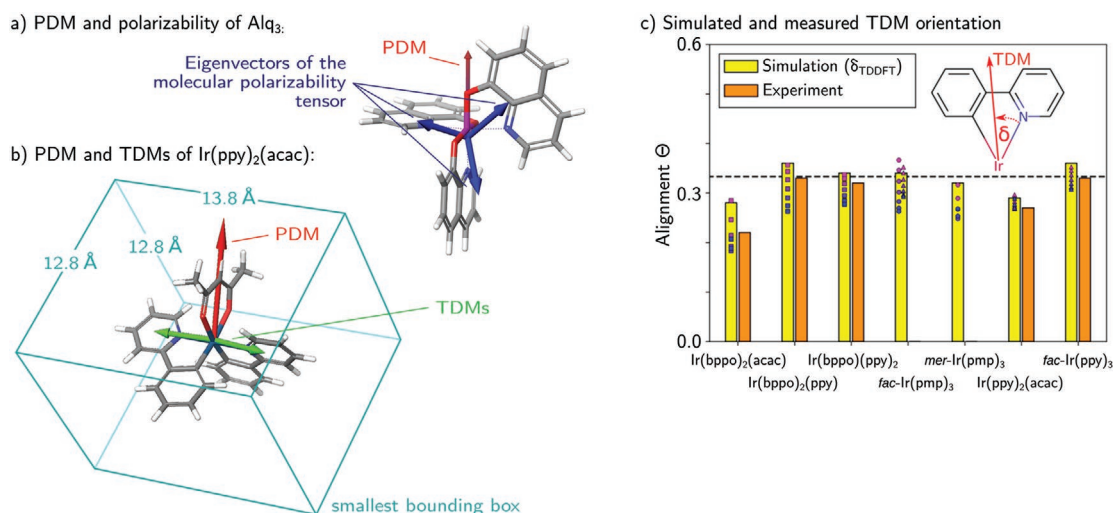


**Figure 3.** Computer simulations. a) The PDM of Alq<sub>3</sub> together with the three eigenvectors of the polarizability tensor of the molecule calculated with DFT at B3LYP and 6-31G\*\* level of theory. b) PDM and the two TDMs with highest probability of the phosphorescent emitter Ir(ppy)<sub>2</sub>(acac) from TD-DFT with the B3LYP functional, the basis dyall-2zcvp and the ZORA hamiltonian. The smallest bounding box of the molecule is calculated to  $a = c = 12.8 \text{ \AA}$ ,  $b = 13.8 \text{ \AA}$ . The calculations in (a) and (b) were executed and visualized with Schrödinger.<sup>[76,77]</sup> c) Correlation between simulation and experiment regarding the orientation of the transition dipole moment of various hetero- and homoleptic Iridium emitters. (Adapted with permission.<sup>[75]</sup> Copyright 2017, American Chemical Society).

there are advances in modeling the deposition process to gain further insights into film morphology and the microscopic driving forces controlling the film formation. These two parts will be discussed separately in following paragraphs.

### 3.5.1. Single Molecule Calculations

An extensive discussion on the correct choice of basis functions, DFT functional or appropriate approximations would exceed the scope of this article and can be found in other publications, text books, or the documentation of the DFT program of choice.<sup>[79–84]</sup> Instead, we want to give an overview over the quantities that can be calculated with TD-DFT and how they help to understand the morphology of organic films. Finally, we also want to mention the limitations of this method and give examples where more sophisticated modeling is required.

**Molecular Structure:** DFT is able to accurately predict the ground state geometry of single molecules, if the basis and the functional are chosen correctly.<sup>[79,80]</sup> This molecular geometry is used for the prediction of all other quantities. Therefore, the convergence to an optimal structure should always be checked before further evaluation of the results. Furthermore, organic molecules offer many rotational degrees of freedom and can exhibit more than one stable configuration in vacuum.<sup>[10,85,86]</sup> In the film, a mixture of these different structures, which can be approximated by a Boltzmann population, will be present.<sup>[85,86]</sup> In order to generalize the information on the molecular structure, for example, for the comparison of the shape of different molecules, the aspect ratio of the smallest bounding box<sup>[62,87]</sup> (see Figure 3b for example) or the eigenvalues of the tensor containing the moments of inertia<sup>[88]</sup> are common parameters.

**Permanent Dipole Moment:** As the optimized geometry contains information about both the position of the atomic cores as well as the electron density, a calculation of the PDM is straightforward. As an example, the PDM of Alq<sub>3</sub> is displayed in Figure 3a. The accuracy of the PDM is nevertheless limited by the fact, that many organic molecules exhibit more than one stable conformer in vacuum.<sup>[85,86]</sup> Furthermore, polarization effects are ignored when looking at an isolated molecule. However, there are developments for taking this into account,<sup>[89]</sup> as will be discussed below.

**Polarizability:** The response of a molecule to an external electric field is described by its polarizability  $\alpha$ , which is a tensor of rank two in general. In the typically applied Born–Oppenheimer approximation, the polarizability can be split into the electronic contribution, that governs the UV–vis region and nuclear relaxation for the IR or Raman part of the spectrum.<sup>[31,71]</sup> Both contributions can be calculated separately. Also, the polarizability is closely related to the structure of the molecule. Alq<sub>3</sub>, for example, with its rather spherical shape, also shows three nearly equal eigenvalues of its electronic polarizability as indicated in Figure 3a.

**Excited State Properties and TDMs:** In addition to the prediction of ground state properties, time-dependent DFT has become a versatile tool to evaluate and predict the excited state behavior of organic molecules.<sup>[84]</sup> In Figure 3b, the transition dipole moments of Ir(ppy)<sub>2</sub>(acac), which are responsible for light emission, are drawn on the structure of the molecule. Emission characteristics like fluorescence decay rates can be

predicted quantitatively. Especially in the context of phosphorescent dyes and TADF emitters, where spin orbit coupling<sup>[11,90]</sup> or second order vibronic effects<sup>[91]</sup> have to be considered, these calculation can become involved and computationally expensive. Nevertheless, these simulations help to optimize and predict promising molecular structures,<sup>[92]</sup> understand the underlying processes during light emission<sup>[90,91,93]</sup> and interpret experimental results.<sup>[11,94]</sup> Only for few TADF molecules, like the so-called multi-resonant emitters, TD-DFT is not able to reproduce the experimental results and a more general treatment of the electrons is required.<sup>[95]</sup>

### 3.5.2. Modeling the Deposition Process

The simulations discussed so far address single isolated molecules in the gas phase. This limits the validity of the calculations as the disordered nature of the film and the effect of the surrounding material is neglected.<sup>[78,96]</sup> There are many examples, however, showing that these effects have to be taken into account in order to explain experimental results.<sup>[78,96–98]</sup> In order to describe these phenomena, a description of the intermolecular interaction and a large number of molecules in the range of a few hundred or even thousands is required. A quantum mechanical treatment of the electrons like in DFT is not possible in this context and might not even be more accurate than classical approximations.<sup>[99]</sup> Instead, the following approaches are used to model the deposition process:

**Coarse Grained Modeling:** In this framework, the molecular fragments are replaced by Lennard–Jones particles. While the intramolecular interactions are governed by stiff bonds between the particles, the intermolecular interaction is modeled by a Lennard–Jones potential between the points mimicking the van-der-Waals interaction. In spite of the relatively strong simplifications of this model, Lyubimov et al. showed that it is able to reproduce the trends of the film morphology.<sup>[100]</sup>

**Monte Carlo Simulation:** As a second approach, Neumann et al., developed a Monte Carlo simulation based on the Metropolis acceptance criterion and an optional simulated annealing step to mimic the vapor deposition process for amorphous organic solids.<sup>[101]</sup> The group applied this technique to study the orientation of phosphorescent Ir-complexes and, as shown in Figure 3c, they successfully reproduced experimental results.<sup>[75]</sup> Furthermore, they extended their simulation protocol by an additional quantum mechanical modeling step taking polarization effects into account.<sup>[102]</sup> Based on this protocol, they were able to reproduce experimental results for the dipole orientation of polar molecules.<sup>[89]</sup>

**Molecular Dynamics:** In this classical approach, the equation of motion for every atom in a simulation box is evaluated and solved based on atom and site specific coefficients, like force constants or bond lengths, for the atomic interaction. The determination of these coefficients, the so-called force field, that governs both the inter and intramolecular interaction, is of crucial importance for reliable calculations.<sup>[99]</sup> Molecular dynamics have been applied to study many morphological phenomena in organic electronics. Emitter orientation of phosphorescent and fluorescent dyes,<sup>[88,103,104]</sup> charge carrier mobility of transport materials<sup>[78,105]</sup> or disorder effects for TADF emitters.<sup>[97,98]</sup>

## 4. Understanding and Controlling Molecular Orientation

As already mentioned in the introductory remarks, orientation effects have been observed in organic optoelectronics over the last 2 decades (or more). However, only in recent years have researchers started to develop a systematic understanding for these phenomena and, thus, laid the foundations for actively controlling and exploiting them in devices.

In 2011, Yokoyama published a seminal review in which molecular orientation of neat layers was related to the shape, or more specifically the aspect ratio, of molecules, as indicated schematically in **Figure 4a**.<sup>[10]</sup> It was found that evaporated layers of certain rod- or disc-like molecules exhibit optical anisotropy, even though the film morphology was amorphous (“glassy”), that is, lacking signs of long-range order. A clear correlation between the aspect ratio of the constituent molecules and the magnitude of birefringence (with non-resonant  $\Delta n$  values up to 0.2) or the order parameter  $S$  (as strong as  $-0.4$  in some cases) could be identified. It was also reported that molecular orientation of neat films can be influenced by the temperature of the substrate during vapor deposition of some of the materials. Remarkably, even a reversal of their orientation from preferentially lying in a film grown at room temperature to standing molecules (film grown at  $110\text{ }^{\circ}\text{C}$ ) was observed.

This manifestation of orientation control by the substrate temperature was thoroughly elaborated by the Ediger group who coined the term “anisotropic molecular glasses” for these materials.<sup>[12,29,108]</sup> In a systematic study of the orientation behavior of prototypical (mostly rod-like) molecules, they could clearly demonstrate that the order parameter  $S$  and the

birefringence  $\Delta n$  of films can be controlled by the ratio of the substrate temperature  $T_s$  and the glass transition temperature  $T_g$  of the deposited material (see **Figure 4b,c**). If  $T_s$  is low enough, molecular orientation saturates at negative  $S$ , that is, horizontal alignment, with the exact value depending on molecular structure. Above a critical value of  $T_s/T_g \approx 0.85$ , however,  $S$  starts increasing and the lying orientation turns into isotropic and even slightly standing, before it becomes fully isotropic ( $S = 0$ ) as  $T_s$  reaches  $T_g$ . As shown in their work, the deposition rate of organic molecules plays a similar role as the substrate temperature, indicating that molecular orientation is kinetically controlled. Specifically, computer simulations have been used to develop a surface equilibration model (see ref. [100]) for vapor-deposited molecular glasses. In essence, molecular orientation is determined at the free surface of a growing film because diffusivity and reorientation in the bulk of a film are orders of magnitude slower than at the surface and are therefore frozen in (see **Figure 4c**). Thus, the thickness of the uppermost “mobile” molecular layers and their orientation determine molecular order in a film as the layer grows thicker and thicker. A potential influence of the substrate soon disappears after a few monolayers. The rate dependence has been demonstrated by Bishop et al., by a variation of the deposition rate of the molecule itraconazole spanning three orders of magnitude.<sup>[109]</sup> For that particular molecule, the relaxation process for orientational motion is found to be more than three orders of magnitude slower in the bulk compared to the surface.

A clear manifestation for this scenario comes from guest–host systems, where instead of the substrate temperature during film growth now the  $T_g$  of the host has been systematically varied.<sup>[110]</sup> As shown in **Figure 5a**, the emitter orientation

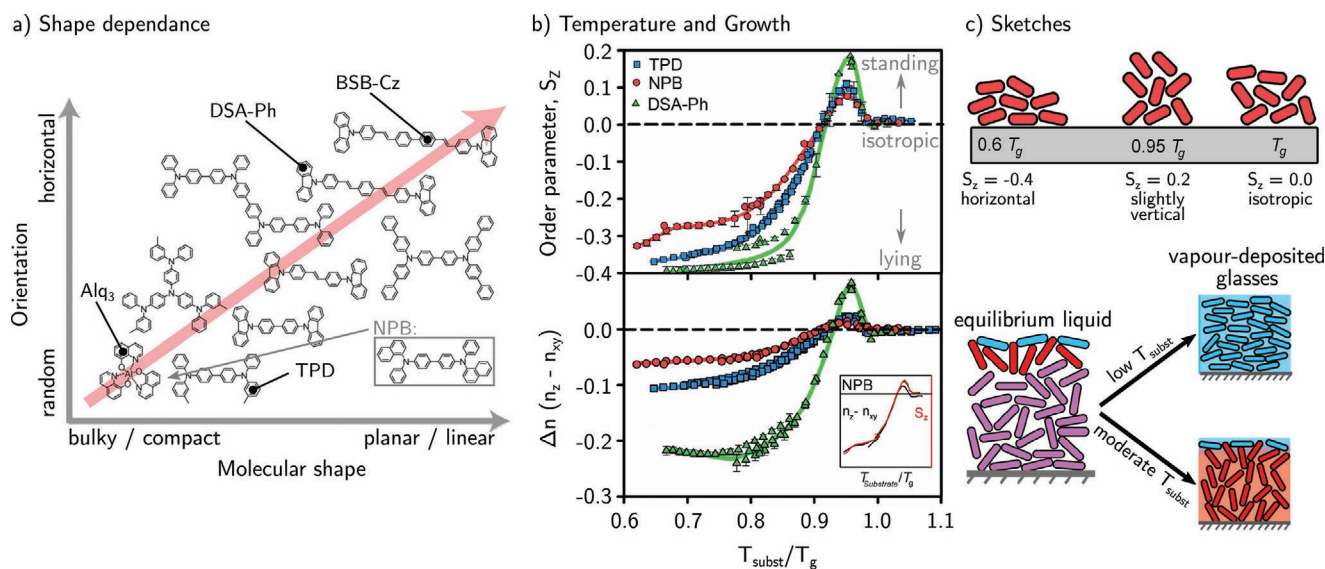


**Figure 4.** Orientation of neat (undoped) organic semiconductors. a) Shape dependence of orientation. The more planar or linear (rod-shaped) the molecules are, the more likely a horizontal or non-isotropic orientation is observed. NPB was not originally included in the reference, but would be situated left to TPD. (Adapted with permission.<sup>[10]</sup> Copyright 2011, Royal Society of Chemistry; permission conveyed through Copyright Clearance Center, Inc.) b) Besides the shape of the molecule, the growth conditions play a crucial role. Given are the order parameter  $S$  as well as the birefringence  $\Delta n$  for different materials with varied deposition temperature. Reproduced with permission.<sup>[106]</sup> Copyright 2015, PNAS. c) Top: Sketch of molecular orientations, their textual description and the according  $S$ -parameter. Adapted with permission.<sup>[106]</sup> Copyright 2015, PNAS. Bottom: Sketch of the molecular orientation inside organic films deposited at high and low substrate temperatures. Reproduced with permission.<sup>[29]</sup> Copyright 2019, American Chemical Society (originally published in and reproduced with permission from ref. [107], Copyright 2017, AIP Publishing).



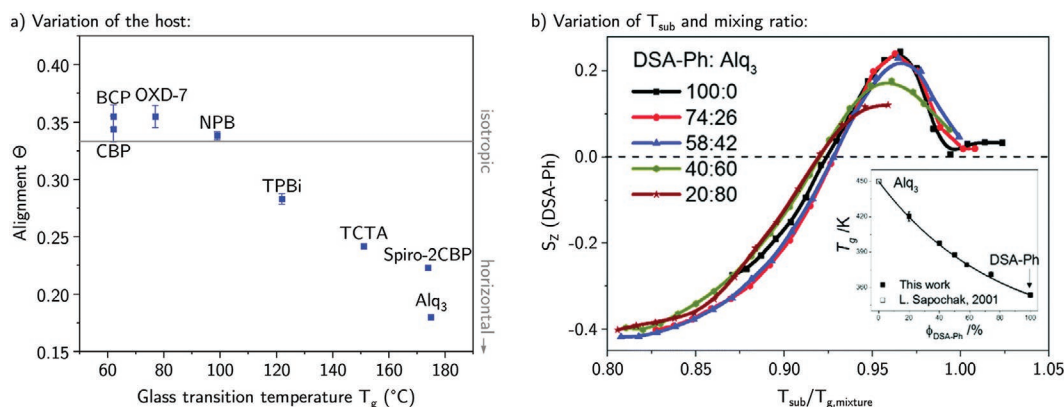


**Figure 5.** Examples for the dependence of the orientation of a guest molecule on the host material, specifically its glass-transition temperature  $T_g$ . In (a), the host material was varied, whereas the guest coumarin-6 stayed constant (Adapted with permission.<sup>[110]</sup> Copyright 2015, American Chemical Society). In (b), both guest and host molecule stayed the same, but instead the substrate temperature during fabrication, as well as the mixing ratio was varied. (Reproduced with permission.<sup>[111]</sup> Copyright 2016, Royal Society of Chemistry (Great Britain); permission conveyed through Copyright Clearance Center, Inc.).

parameter  $\Theta$  of the small molecule Coumarin-6 doped at small amount into different host materials nicely follows the same  $T_s/T_g$  trend as in the case of neat films, where  $T_s$  is varied. Furthermore, a qualitatively similar behavior is observed if two materials with different glass transition temperatures are mixed at varied ratio, such that the  $T_g$  of the blend changes in a systematic manner, see Figure 5b.<sup>[111]</sup>

All this indicates that molecular orientation in vapor-deposited thin films is kinetically controlled, however, the most important prerequisite still being shape anisotropy, that is, the aspect ratio in the geometry of molecules. But this also raises the question if—in addition to the van-der-Waals interaction that determines the preferred orientation of a molecule upon landing on the film surface—other microscopic interactions can influence molecular orientation as well. This leads us to polar molecules, where electrostatic dipole–dipole interactions are to be considered. It is worth a note, however, that spontaneous

orientation of organic molecules is so far only observed in vacuum-processed films, as has been shown in a comparison of different deposition techniques for various Ir-complexes.<sup>[112]</sup>

As detailed in Sections 2 and 3, a non-vanishing net alignment of molecules with finite PDM leads to surface potentials and interface charges that can be probed electrically.<sup>[30]</sup> Figure 6a shows a compilation of measured GSP data for molecules with different magnitudes of their PDM. In general, there is an overall trend of increasing layer polarization with increasing PDM, as expected. But there are some details that deserve a comment: First, a quantitative analysis of the GSP magnitude shows that only a small fraction, typically less than 10%, of the PDMs are actually vertically aligned, considering the simple picture of vertical in contrast to isotropic orientation.<sup>[51,113,114]</sup> Of course, this could as well be explained by an almost random orientation distribution of the PDM vectors with just a small net preferential alignment of in turn higher probability. However,

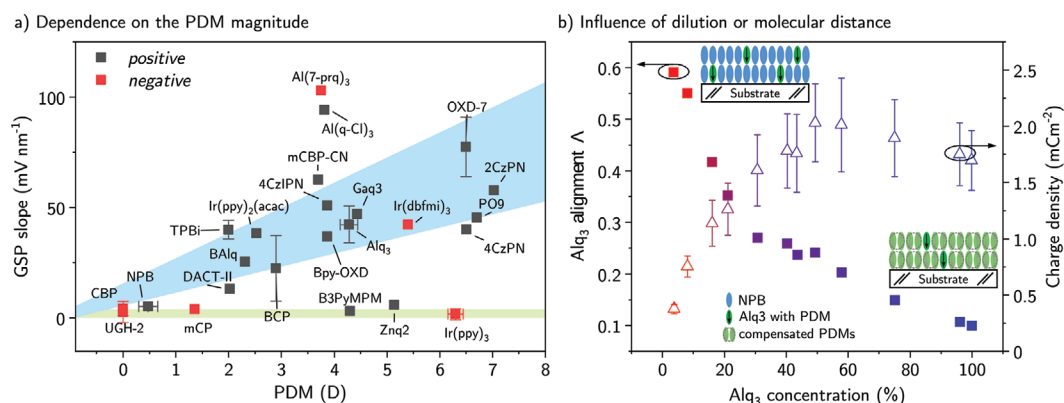


**Figure 6.** Influence of the permanent dipole moment and the molecular doping on the resulting GSP. a) Overview following the scheme of Osada et al.<sup>[61]</sup> linking measured GSP and calculated PDM magnitude. The green bar denotes “unpolar” films, the blue corridor the usual spread of resulting GSP for polar films. Most of the known molecular species exhibit positive—or only slightly negative—GSP. So far, only two (Al(7-Prq)<sub>3</sub> and Ir(dbfmi)<sub>3</sub>) are clearly oppositely aligned resulting in strong negative GSP. (Adapted with permission.<sup>[61]</sup> Copyright 2018, Elsevier. Additional datapoints were added with data from refs. [30,41,51,60,62,86,115]). b) Concentration dependence of the GSP and orientation factor measured on NPB:Alq<sub>3</sub> devices. Higher degree of orientation is observed for larger distances between the Alq<sub>3</sub> molecules in diluted film as indicated in the sketches. (Adapted under the terms of the CC-BY 4.0 license.<sup>[113]</sup> Copyright 2016, The Authors, published by AIP; combination of two figures from the original work).



it could also indicate that a large fraction of molecular PDMs cancel each other by anti-parallel alignment, as this is the energetically most favorable configuration. Second, the vast majority of polar molecules studied so far exhibit positive GSP, that is, their PDMs point away from the substrate to the vacuum side. And, third, the degree of PDM alignment can be largely enhanced by diluting the polar species in a non-polar host, as shown for Alq<sub>3</sub> doped into NPB in Figure 6b. It is found that up to 60% of the PDMs of Alq<sub>3</sub> molecules are vertically aligned if it is highly diluted ( $c < 5$  mol%) in the non-polar NPB.<sup>[113]</sup> Similar observations have been reported for other polar molecules, like Ir(ppy)<sub>2</sub>(acac)<sup>[51]</sup> or TPBi,<sup>[114]</sup> as well.

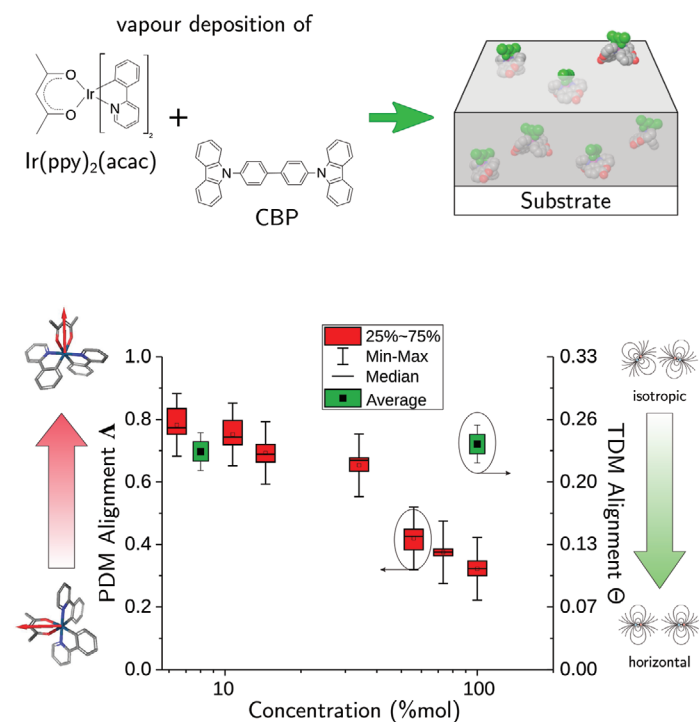
This can be considered as clear manifestation of electrostatic dipole–dipole interactions acting on the alignment process of polar molecules. As explained in detail in ref. [30], because of their strong distance dependence with  $V_{\text{dipole-dipole}} \propto r^{-3}$ , mutual compensation effects play an important role in neat films, however, they can be significantly reduced by dilution in guest–host systems. Furthermore, it has recently been shown that guest–host interactions can even promote alignment for particular polar guest–host systems used in TADF OLEDs, where a subtle interplay of PDM compensation and TDM alignment was observed.<sup>[86]</sup>

This directly brings us to a holistic treatment of both properties: optical TDM and electrical PDM alignment. The family

of phosphorescent emitter complexes offers a unique opportunity for such studies because of its octahedrally coordinated ligand sphere around the central Ir atom. Surprisingly, in spite of their almost spherical geometry, some of them show TDM alignment that boosts light-outcoupling from OLEDs significantly.<sup>[54,116]</sup> Initially, only heteroleptic complexes, like the one shown in Figure 7a, were thought to exhibit this feature and the proposed orientation mechanism was based on their chemical asymmetry.<sup>[117]</sup> The non-aromatic ancillary (acac)-ligand was suggested to orient toward the free surface of a co-deposited film, and this happened more or less independent of the used matrix material.<sup>[110]</sup>

Owing to their specific geometry, with the C2 pseudo-symmetry axis in the direction of the ancillary ligand being also the direction of the PDM of the molecule, and the TDMs on the other two emissive ligands being almost perpendicular to the symmetry axis, these complexes were used for a combined study of both TDM and PDM alignment.<sup>[51]</sup> As shown in Figure 7a, at low emitter concentration ( $c < 10\%$ ), as typically used in OLEDs, both vectors are preferentially aligned—the PDM vertically and the TDMs horizontally, which directly proved the suggestion by Jurow et al., for the first time.<sup>[117]</sup> However, as the concentration is increased, the PDMs gradually lose their preferred alignment. Again, this indicates that electric dipole–dipole interactions between PDMs tend to

#### a) Optical and electrical alignment for heteroleptic compounds



#### b) Orientation of homoleptic Ir-Complexes (e.g. Ir(dbfmi)<sub>3</sub>)

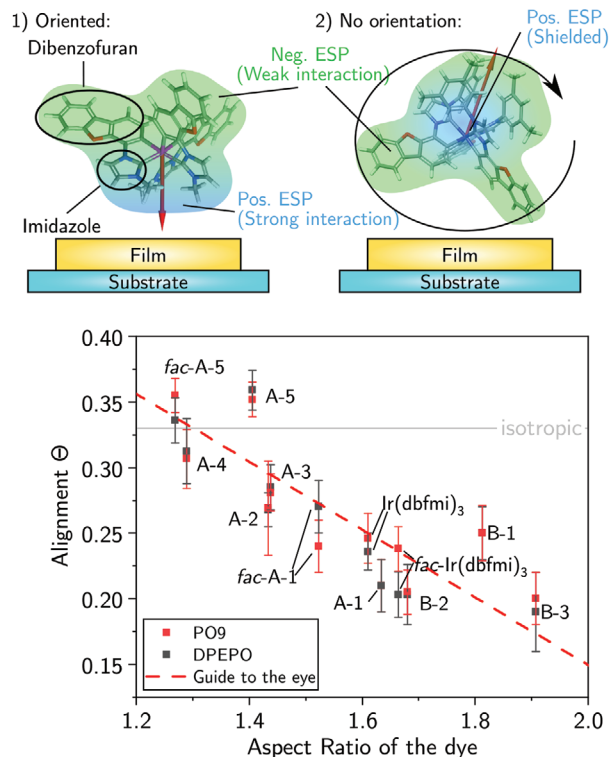


**Figure 7.** Molecular orientation of iridium complexes. a) Electrical and optical alignment of heteroleptic Ir(ppy)<sub>2</sub>(acac). Similar to the case of NPB:Alq<sub>3</sub> in Figure 6b, lower concentrations of Ir(ppy)<sub>2</sub>(acac) in CBP show higher PDM orientation, though it is not detectable in ADPL. (Sketch adapted with permission.<sup>[112]</sup> Copyright 2016, American Chemical Society. Graph reproduced with permission.<sup>[51]</sup> Copyright 2018, American Chemical Society). b) Alignment mechanism for homoleptic Iridium carbene complexes depending on the distribution of the ESP. The graph shows the measured TDM orientation in dependence to the aspect ratio of the Ir-dye. (Adapted and reproduced from ref. [62] with special permission from the American Chemical Society, further permissions related to the material excerpted should be directed to the ACS).

form aggregates with antiparallel alignment and no net dipole moment, as it was found already for the above-mentioned SOP studies. Nevertheless, the TDM alignment is still preserved. This is possible because of the special geometry of these  $\text{Ir}(\text{C}_6\text{N}_2)(\text{acac})$  complexes, with PDM and TDMs being perpendicular to each other, and should not be presumed to hold true for heteroleptic complexes in general.

Computer simulations confirmed this view and, specifically, revealed that van-der-Waals interactions between the underlying substrate or film material and vapor-deposited emitter molecules determine their preferred orientation upon arrival at the film surface.<sup>[75]</sup> This directs conjugated ligands to interact stronger with the underlying host molecules and, thus, determines the orientation of the complex. Accordingly, homoleptic complexes with three identical ligands—all of them aromatic—were predicted to have no preferential alignment.

However, in view of later studies, this notion has been revised meanwhile as quite a number of such Ir emitter complexes with three identical ligands were reported to have non-isotropic orientation.<sup>[118]</sup> In a recent work (see Figure 7b), Schmid et al., have performed a systematic variation of the ligand substitution pattern of homoleptic Ir-carbene complexes and found that TDM alignment can be tuned by the geometric aspect ratio of the molecules.<sup>[62]</sup> Furthermore, they could identify specific regions of the molecules that interact preferentially with the surface of a growing vapor-deposited film. Nevertheless, the exact nature of the interaction and the detailed alignment mechanism are still subject of ongoing research. Such knowledge may allow designing tailor-made complexes with even stronger alignment in the future. We also want to note that Pt complexes with their square-planar ligand configuration are distinctly different from Ir complexes and, thus, have their own design rules for alignment. Interestingly, for  $\text{Pt}(\text{fppzc})_2$  with its special metal-metal-to-ligand CT character, almost completely horizontal TDM alignment was reported.<sup>[119]</sup> However, so far, they are much less important in organic optoelectronics.

Finally, the booming class of TADF OLED emitters deserves some separate consideration. As compared to phosphorescent materials with their frequently close to spherical structures, they offer much larger freedom in their design.<sup>[120]</sup> Since their working mechanism to harvest triplet excitons via reverse intersystem crossing is based on an intramolecular charge-transfer state, these TADF emitters typically have spatially separated regions on the molecule with donor (D) and acceptor (A) character.<sup>[91]</sup> Often, this is reached by linear D–A structures with a twist between both parts of the molecule. Such molecules tend to have both their TDMs and PDMs parallel to the main axis of the molecule. Thus, if the overall geometry is rod-like or disk-like, they can be preferentially aligned by suitable film growth conditions. Furthermore, these structures can be made even more elongated if a D–A–D (or, equivalently, an A–D–A) motif is used.

As shown in **Figure 8a**, Komino et al.,<sup>[121]</sup> have used such a TADF emitter to demonstrate perfectly horizontal TDM alignment if the film was grown on a cooled substrate ( $T_s = 200\text{ K}$ ). On the other hand, isotropic TDM orientation was obtained for high temperature growth ( $T_s = 370\text{ K}$ ) or post-growth annealing at comparably high temperatures. Other studies have revealed that the aspect ratio of the TADF emitter molecule plays a crucial role (Figure 8b)<sup>[87]</sup> and that the TDM orientation of a given

emitter can be controlled by the  $T_g$  of the host (Figure 8c).<sup>[86]</sup> The latter example again manifests the fact that elongated symmetric (in this case A–D–A) molecules are inherently oriented stronger horizontally than the shorter asymmetric D–A structures. It has also been argued that the presence of a PDM in asymmetric molecules could play a role as well, for example by electric dipole–dipole interactions with the host molecules, which are typically polar species due to the CT character of excited states in TADF emitters.<sup>[38,86]</sup> However, this issue is still subject of ongoing investigations.

To conclude this section, recent years have seen considerable progress in understanding and growing maturity in actively controlling molecular orientation for organic optoelectronics. Remarkably high degrees of orientation can be achieved in such vapor-deposited anisotropic molecular glasses. The most important prerequisite for this behavior is, undoubtedly, the shape anisotropy of the constituent molecule itself.<sup>[10]</sup> However, since film growth by physical vapor deposition often is a kinetically controlled process far from equilibrium, other factors like the growth rate or the substrate temperature and the glass temperature of the surrounding host matrix play a decisive role as well.<sup>[12]</sup> Beyond these general features, details of the molecular structure do, of course, also matter as they may induce local interactions—be it electrostatic potentials or H-bonding—which may favor certain molecular arrangements relative to each other.<sup>[118,122]</sup> Predicting such behavior by (ab initio) molecular simulations is still challenging, in part due to system size and the required computational cost, and also due to limited knowledge of all the relevant interactions.<sup>[75,89]</sup> Nevertheless, the obtained knowledge has already very successfully been used in device applications, which will be discussed in the following section.

## 5. Device Relevance of Molecular Orientation

Besides the mechanisms of molecular orientation and possible measurement techniques, its impact on device performance shall be discussed. For OLEDs, the orientation of the emitting dipoles largely influences the light outcoupling efficiency, which will be addressed in Section 5.2. Additionally, the influence of molecular orientation on charge transport must not be neglected.

### 5.1. The Influence of Molecular Orientation in Transport Layers

#### 5.1.1. Dependence of Charge Carrier Mobility on Molecular Orientation

The charge transport activation energy between two adjacent molecules is largely influenced by the amount of overlap of their  $\pi$ -electron systems.<sup>[123]</sup> Accordingly, the average orientation of molecules in relation to each other as well as the direction of travel defines the charge carrier mobility of a thin film. This was impressively demonstrated by Yokoyama et al., who studied electron and hole mobilities of the rod-shaped small molecule organic semiconductor BSB-Cz in films grown at different substrate temperatures,<sup>[10]</sup> see **Figure 9a**. Both electron

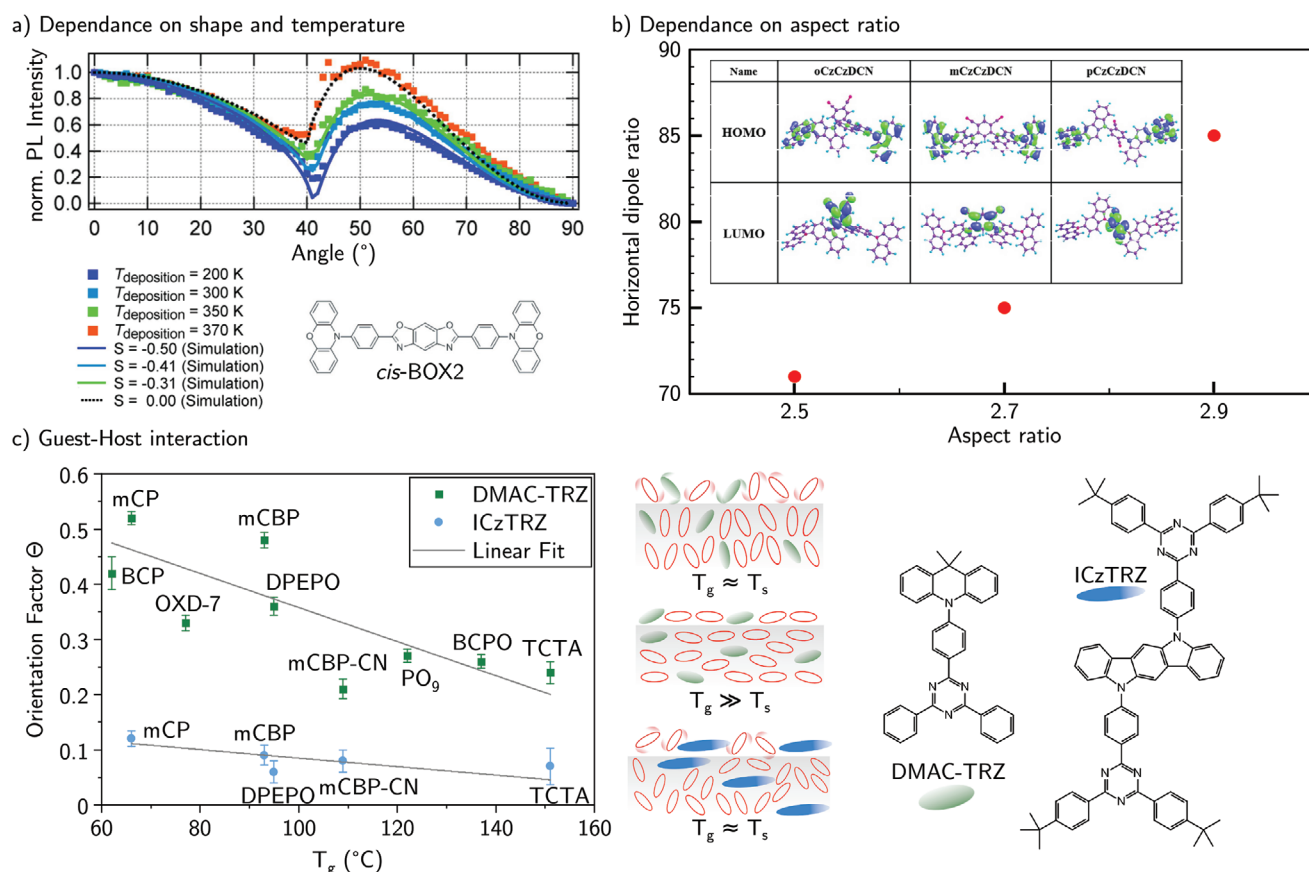


**Figure 8.** a) ADPL measurement data for 6% *cis*-BOX2 in CBP in dependence of the deposition temperature. Given is also a corresponding simulation of the *S*-parameter showing the transition from horizontal to isotropic orientation between 200 to 360 K. (Reproduced with permission.<sup>[121]</sup> Copyright 2016, AIP Publishing.) b) Correlation of the aspect ratio of the TADF emitters OCzCzDCN, MCzCzDCN, and pCzCzDCN (shown in the inset) with the ratio of horizontal dipoles. (Reproduced with permission.<sup>[87]</sup> Copyright 2017, Elsevier.) c) Dependence of the emitter orientation factor on the glass transition temperature of the host. Green squares correspond to the TADF emitter DMAC-TRZ, blue dots denote the emitter ICzTRZ. On the right, a schematic illustration of the thermal mobility of the host molecules on the orientation of the guest as well as the Lewis structures of the two emitters is given. (Reproduced under the terms of the CC-BY 4.0. license.<sup>[86]</sup> Copyright 2020, The Authors, published by Frontiers in Chemistry).

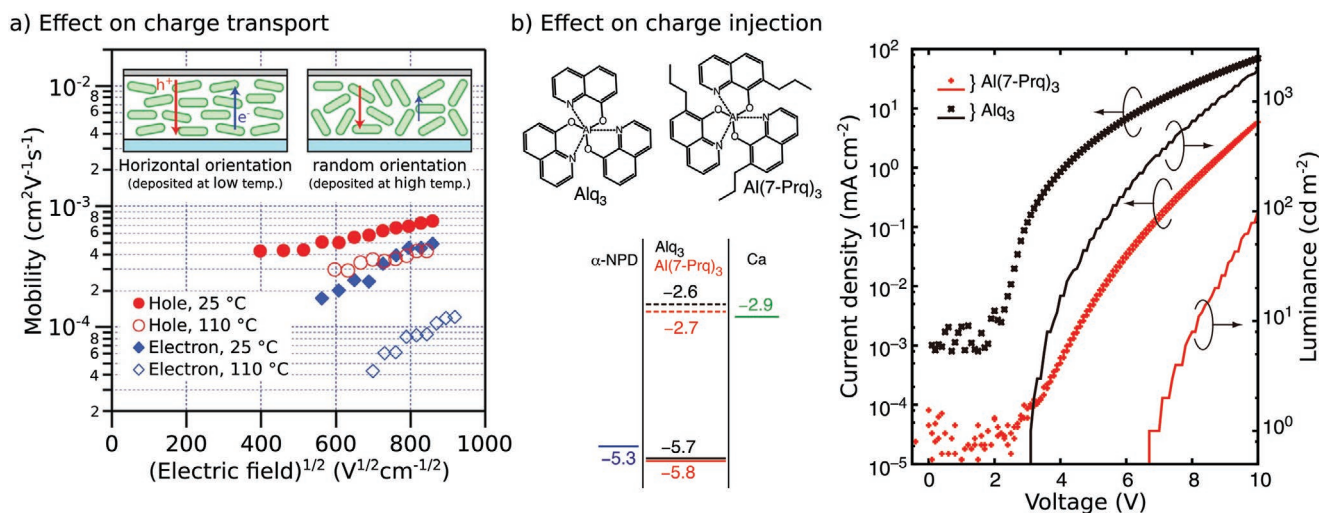


**Figure 9.** a) Hole and electron mobilities of the linearly shaped molecule BSB-Cz (top most structure in Figure 4a). Both carrier types show higher mobilities in the case of horizontal alignment (deposited at 25°) with a difference of up to one order of magnitude for electrons. Reproduced with permission.<sup>[10]</sup> Copyright 2011, Royal Society of Chemistry (Great Britain); permission conveyed through Copyright Clearance Center, Inc.; originally published in and reprinted from ref. [124] with permission of Wiley-VCH, Copyright 2010.) b) Charge injection into organic films in dependence of the direction of the film polarization. With similar energy levels, Al(7-prq)<sub>3</sub> as ETL orients its PDM opposite to Alq<sub>3</sub>, effectively blocking charge injection of electrons into the device. (Reproduced with permission.<sup>[60]</sup> Copyright 2013, AIP Publishing).

and hole mobility are significantly larger, by up to one order of magnitude, if the film is grown at room temperature, compared to elevated temperatures of 110°. The reason lies in the tendency for BSB-Cz to grow with preferentially horizontal alignment at lower temperatures, leading to more pronounced  $\pi$ - $\pi$ -stacking in the out-of-plane direction, in which the current is applied. At elevated temperatures, however, more random orientation prevails, hindering charge transport.

### 5.1.2. Additional Influence of a GSP on Charge Injection

At the contact between metallic electrodes and the organic layers, the build-up of interface dipoles affects the energy alignment and thus the injection barriers into the organic material.<sup>[125]</sup> Accordingly, artificially introduced self-assembled dipole monolayers can be utilized to tune the contact barriers.<sup>[126]</sup> However, if polar molecules show SOP upon film growth, a direct effect of the resulting film polarization on charge injection has also been found. Starting from a prototypical fluorescent OLED stack based on NPB and Alq<sub>3</sub>, Noguchi et al., reported a decrease in device current and luminance by more than one order of magnitude, when Alq<sub>3</sub> is substituted by Al(7-Prq)<sub>3</sub>,<sup>[60]</sup> as seen in Figure 9b. Although optically and energetically similar, the addition of three propyl-groups to Alq<sub>3</sub> strongly influences the orientation of the PDM upon film growth: Al(7-Prq)<sub>3</sub> shows a reversed orientation of its PDM compared to Alq<sub>3</sub>, eventually yielding a reversed GSP. As a result, the OLED device current is drastically reduced if Al(7-Prq)<sub>3</sub> is used. They concluded, that a positive charge at the NPB/Al(7-Prq)<sub>3</sub> interface hinders hole accumulation and also suggested a high contact resistance for electron injection into the Al(7-Prq)<sub>3</sub> layer resulting from the negative charges at the cathode.<sup>[60]</sup> On the other hand, electron injection into Alq<sub>3</sub> is improved due to stabilization of the anion state (electron) at the Alq<sub>3</sub>/cathode interface leading to a reduction in injection barrier, which has later been shown by Kinjo et al., using photo-electron spectroscopy.<sup>[127]</sup> A drift-diffusion approach presented by Altazin et al., also successfully reproduced the effect of differently oriented GSP by mimicking the presence of immobile interface charges in simulation.<sup>[128]</sup>

A similar effect can also be achieved for hole injection at the anode side. Recently, Hofmann et al., reported a method suitable for modifying the injection barrier into the HTL using the concept of dipolar doping.<sup>[129]</sup> For this purpose, a former unpolar molecule like NPB is doped with the polar species Alq<sub>3</sub>, which leads to a tunable GSP in the respective layer.<sup>[113,129]</sup> Although the doped HTL shows lower mobility, a reduction of the interface dipole at the anode/NPB:Alq<sub>3</sub> interface leads to an overall lower injection barrier, with currents increasing by one order of magnitude at low doping ratios.

### 5.1.3. Impact of Optical Anisotropy of the Transport Layers on Light-Outcoupling

Besides the effects of a preferential alignment of the PDM on charge injection and transport in the organic layer, optical anisotropy of the film has an impact on the light propagation as well. In optical simulations of a generic bottom emitting OLED,

Callens et al., showed that birefringence of the transport layers influences the fraction of light leaving the organic light emitting diode.<sup>[34]</sup> They found, that the impact of a birefringent ETL is generally larger compared to the effect of an anisotropic HTL, as this material is next to the reflective cathode in their device layout. Thus, negative birefringence of the ETL that corresponds to horizontal alignment of the molecules is favorable for light outcoupling from the device stack. Based on these results, Schmid et al., also studied the effect of anisotropic transport layers on OLED efficiency.<sup>[35]</sup> In that work, similar optical simulations were carried out with the actual refractive indices and the isotropic average refractive index  $n_{\text{iso}}$  that can be calculated according to

$$n_{\text{iso}} = \sqrt{\frac{1}{3}(2n_o^2 + n_e^2)} \quad (23)$$

from the ordinary and extraordinary refractive index ( $n_o$ ,  $n_e$ ) of the material. The efficiencies achieved in this study with doped transport layers and from other devices published previously<sup>[130]</sup> exceed the values predicted from the isotropic optical constants. This underpins that devices benefit from anisotropic transport layers.

## 5.2. Emitter Orientation in OLEDs

The most prominent example where molecular orientation is of paramount importance for the functioning and efficiency of the device are, probably, organic light-emitting diodes. It was realized early on that polymer LEDs may exhibit some degree of alignment of their conjugated backbones during the film formation process from solution, be it by spin-coating, blade-coating, or other techniques where shear forces act on the chain-like macromolecules, thus giving them a preferential in-plane alignment.<sup>[5]</sup> Under specific conditions, for example, film stretching or templating by rubbed substrates, it was even possible to achieve preferential alignment along one specific direction within the film plane so that polarized light emission could be observed.<sup>[15]</sup> However, vapor deposition of small molecules, and specifically dye-doped guest-host systems for the emissive layer of an OLED, was initially considered to yield random orientation of molecules and their TDMs. The more surprising was the observation of predominantly horizontally aligned TDMs in both fluorescent and phosphorescent emissive layers about 10 years ago.<sup>[54,131]</sup> The latter came particularly unexpected because these phosphorescent metal-organic complexes were considered to be rather bulky without shape anisotropy.

Nevertheless, it was immediately realized that emitter orientation holds great potential for improving light-outcoupling of OLEDs, which was considered to be the remaining challenge at that time. This is visualized in Figure 10a, where simulations of the maximum external quantum efficiency of an OLED are shown as function of the emitter's quantum yield and its TDM orientation. Note that  $\Theta_h$  in this case denotes the fraction of horizontal dipoles, whereas it was the fraction of vertical ones in our previous definition; but they are easily converted:  $\Theta_h = 1 - \Theta_v$ . Compared to the isotropic case with an EQE of about 25% for the homoleptic phosphorescent



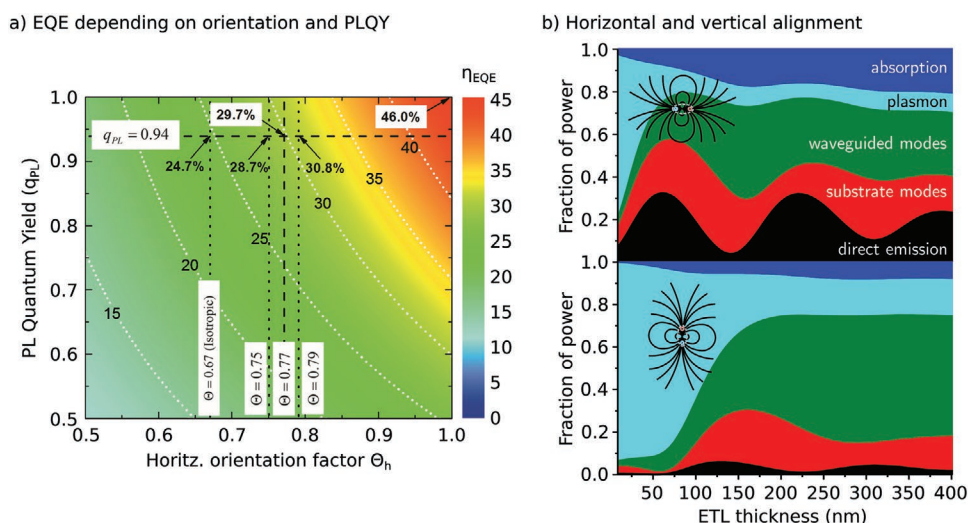


**Figure 10.** a) Simulations of the maximum external quantum efficiency of an OLED given as function of the emitter's quantum yield and the TDM orientation. Note that  $\Theta_h$  is the fraction of horizontal dipoles with  $\Theta_h = 1 - \Theta_v$ . Adapted with permission.<sup>[130]</sup> Copyright 2013, Wiley-VCH (altered to a color image). b) Simulation of the fraction of power emitted into different modes depending on the thickness of the ETL. Only the black portion is emitted directly and leaves the OLED, where the majority of the power is "trapped" or re-absorbed. The situation dramatically worsens for vertical emitter alignment (bottom part). Reproduced with permission.<sup>[11]</sup> Copyright 2017, American Physical Society.

emitter Ir(ppy)<sub>3</sub>, the partially aligned Ir(ppy)<sub>2</sub>(acac) yields almost 30%. And for fully horizontally aligned TDMs and perfect PL quantum yield (PLQY) the EQE could in principle reach more than 45%—without any extra means of light-outcoupling enhancement.

The underlying physics is visualized in Figure 10b, though not for exactly the same stack as in part a. It shows the fraction of power going into different optical channels of the OLED microcavity. For plane glass substrates, only the direct emission is accessible, while the use of an index-matched half-ball lens allows extracting the substrate modes as well. Extraction of waveguided modes and plasmons is rather costly as this requires more or less complex patterning of the whole layer stack.<sup>[36,132,133]</sup> However, as shown in the graph, a rather cheap but nonetheless highly effective way of directing more light into the directly emitted fraction is by aligning the emissive TDMs horizontally. It is also instructive to compare horizontal and vertical alignment as function of layer thickness, which in this case is essentially the distance from the emissive dipole layer to the metallic cathode where interference of forward and backward propagating waves is generated. Owing to different phase shifts upon reflection, however, the thickness variation between horizontal and vertical dipoles is complementary. Thus, it is impossible to find a thickness where both exhibit a maximum of direct emission, which in turn means that vertical TDMs are a loss for OLED efficiency.

Meanwhile, emitter orientation is an established tool to boost OLED efficiency.<sup>[11]</sup> Researchers have developed design rules for its exploitation in the different emitter families. Fluorescent blue emitters are still being used as stable long-lived material in commercial RGB displays, in spite of their inherent limitation of non-emissive triplet states. But as exemplary shown in ref. [134] they often have exceptionally high degree of horizontal TDM alignment and sometimes even harvest part of the dark triplets, for example by delayed fluorescence via triplet fusion, to yield EQEs of 10% or even beyond. Phosphorescent emitters

are state of the art for the green and red part of the visible spectrum, with EQEs reaching up to 30% and sufficiently long operational lifetimes. But there may still be room for improvement by designing emitter molecules with intrinsically better alignment than the currently achieved 80% horizontal TDMs.<sup>[118]</sup> Targeting blue emission with phosphorescent materials remains challenging because the high energy gap hosts that are required show inherent stability issues. That is why TADF emitters and related concepts, like hyperfluorescence, are currently booming.<sup>[91,120]</sup> Their often-large shape anisotropy makes them ideal candidates for horizontal TDM orientation. But their complex photophysics seems to require a more sophisticated view on alignment including other aspects of molecular orientation, for example, polarizability, polarity, and polarization, as well.

## 6. Open Issues

So far in this review, we have discussed the benefits of anisotropic molecular orientation—be it predominantly horizontal TDM orientation for light absorption and emission, preferentially vertical PDM orientation for charge injection or the corresponding packing motifs of molecules for enhanced in-plane or out-of-plane charge carrier mobility, respectively. However, as has been shown, for example, in a work by Adachi et al.,<sup>[135]</sup> charge transport can also be improved if molecules are more densely packed in a film that is grown on substrates heated close to the  $T_g$  of the material (specifically,  $T_s/T_g \approx 0.75$ ), thereby losing much of its orientational anisotropy. Typically, such changes of molecular orientation toward a "glassier" film morphology are accompanied by a subtle increase of the mass density of the order of 1% to 2%, only. However, due to the exponential dependence of electronic wave function overlap on intermolecular distances this seems to be sufficient for sizeable mobility improvements. Thus, there is apparently some

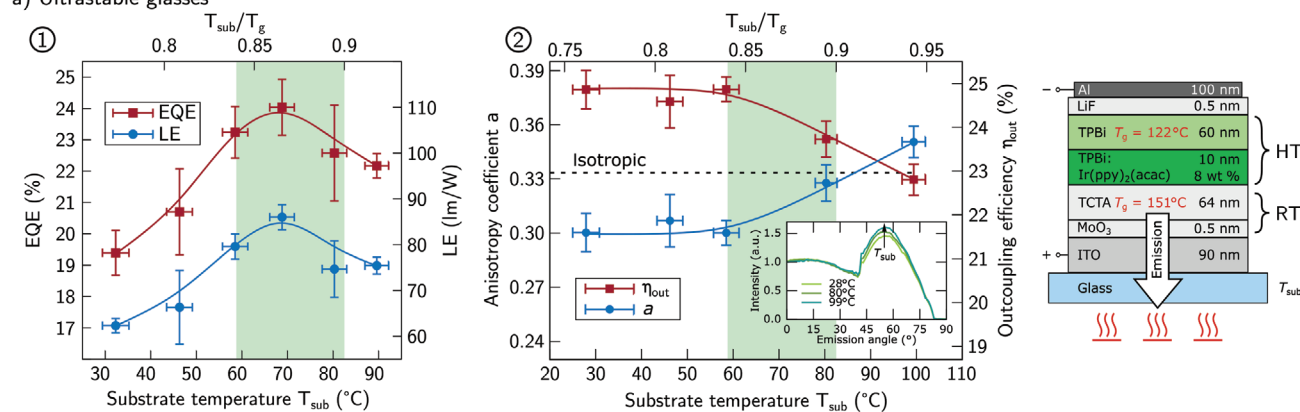


trade-off between achieving the highest degree of anisotropic molecular orientation and the closest packing of molecules that critically depends on the film growth conditions.

Recent investigations have shown, that such compromises have to be made not only in terms of charge transport layers in devices but for the emission layer of OLEDs as well. The group of Reineke has proposed the concept of ultra-stable molecular glasses,<sup>[136]</sup> that is, films grown at  $T_s/T_g \approx 0.85$ , for phosphorescent OLEDs containing a heteroleptic complex  $\text{Ir}(\text{ppy})_2(\text{acac})$  as emitter molecule as well as the polar species TPBi as host material and electron transport layer (see Figure 11a). Both,  $\text{Ir}(\text{ppy})_2(\text{acac})$  and TPBi, are known to exhibit anisotropic molecular orientation—the former of its TDMs leading to better light outcoupling, the latter of its PDMs leading to a GSP—if the device is grown on a substrate kept at room temperature. However, if the substrate is heated during film growth, yielding so-called ultra-stable molecular glasses, OLEDs with better

efficiency and longer lifetime are obtained. This is even more remarkable because the emitter molecules in the heated device lose their advantage of improved light outcoupling by preferentially horizontal TDM orientation. The group of Reineke assigned the overall better performance of the ultra-stable glass OLED to denser packing of molecules resulting in less non-radiative pathways in the light-emitting guest-host system.<sup>[136]</sup> The effect of SOP in the TPBi electron transport layer was initially not considered. Only recently, the group of Holmes disentangled the different effects of TDM orientation in the emission layer and PDM orientation in the electron transport layer and, specifically, how they are affected by substrate heating.<sup>[137]</sup> As shown in Figure 11b, they assigned the increase of the OLED efficiency with higher substrate temperature to a reduction of the GSP of TPBi and, concomitantly, less exciton quenching by accumulated charges in the emission layer. Such triplet-polaron quenching is known to affect the efficiency of OLEDs under

#### a) Ultrastable glasses



#### b) Quenching

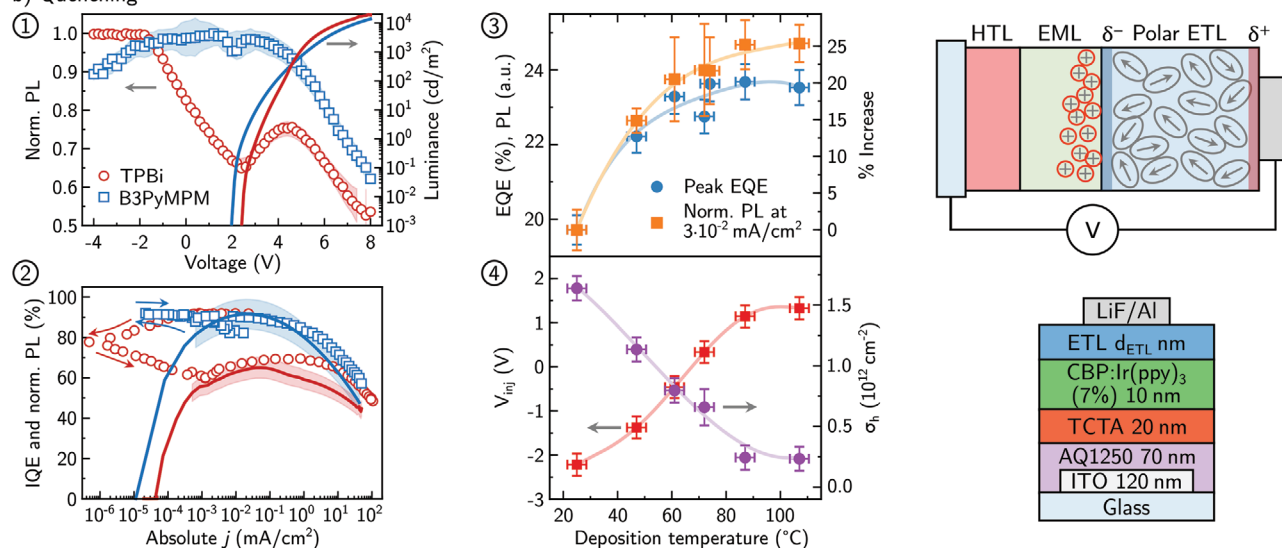


**Figure 11.** Tradeoff between orientation, stability, and quenching. a) Grown at substrate temperatures near  $0.85 \cdot T_g$ , the mixture of  $\text{Ir}(\text{ppy})_2(\text{acac})$  and TPBi forms ultrastable glasses with higher EQE, despite the lower outcoupling factor due to less preferable alignment. In the OLED stack, ETL and EML are processed at elevated temperatures, where the remaining layers are grown at room temperature. (Reproduced under the terms of the CC-BY 4.0 license.<sup>[136]</sup> Copyright 2018, The Authors, published by the American Association for the Advancement of Science). b) A reduction of the GSP in the TPBi leads to less accumulated charges in the EML. This reduces the TPQ rate in the OLED, which in turn boosts the EQE, despite the less favorable TDM orientation. (Reproduced under the terms of the CC-BY 4.0 license.<sup>[137]</sup> Copyright 2020, The Authors, published by the American Association for the Advancement of Science).

forward current flow, however, in this case it is found to play an important role already at reverse bias where no net charge carrier flow occurs. Similar observations were reported also in photoluminescence experiments on a fluorescent emitter doped into an  $\text{AlQ}_3$  matrix showing the GSP effect.<sup>[138]</sup> In another study, the Adachi group investigated mixtures of donor- and acceptor-type molecules, that is, so-called exciplex-forming active layers in OLEDs as well as solar cells and revealed complementary pros and cons with respect to the use of materials exhibiting GSP.<sup>[139]</sup>

Apparently, the effect of SOP deserves further investigation. And the answer to the question whether or not such materials showing orientational order of their PDMs are beneficial in organic optoelectronic devices is more involved. For example, it is well known that TADF emitters require a polar host matrix to enable efficient reverse intersystem crossing from their dark triplet excited state to the emissive singlet CT state. But it is still not clear what effect (partial) alignment of the host's (and/or the guest's) PDMs might have on device performance. After all, it may not only be necessary to make a wise selection of materials for different functional layers in a multi-layer optoelectronic device, but also to tune their orientational alignment by suitable preparation conditions.

Finally, it is of course instructive to look for applications that would not be possible without the unique features of molecular orientation. One historic example is the well-known liquid crystals that have paved the way to a new disruptive display technology starting its success to the nowadays ubiquitous flat computer and television screens from the 1990s on. Another very recent example of an application that is enabled only by molecular orientation are energy harvesting devices, like the one shown in **Figure 12**. It uses an organic layer showing SOP of molecules with PDM, like  $\text{AlQ}_3$  or TPBi that resemble an electret because of their GSP.<sup>[140]</sup> In such a plate-capacitor device, mechanical oscillations induce an electrical current that can perform work in the external circuit. Although the achieved currents are still moderate, it may open a new view on molecular semiconductors to exploit their unique orientational properties and connects to other fields, such as piezo- or ferroelectricity as well.

## 7. Conclusion

Molecular orientation is a key feature in organic optoelectronics, even though these thin-film structures usually lack pronounced long-range order and are, therefore, typically considered to be amorphous. However, in view of recent studies reviewed in this text, they should rather be considered as anisotropic molecular glasses. These anisotropies are manifested in different macroscopic observables such as optical birefringence, non-isotropic light absorption and emission as well as macroscopic dielectric polarization, just to name a few of them. More importantly, as the most recent work has shown, they are often interlinked. For example, polar transport and emitter materials for OLEDs typically feature spontaneous orientation polarization as well as preferential alignment of their transition dipole moments. While the latter is advantageous for coupling out more of the produced light, the former can induce quenching of the excited

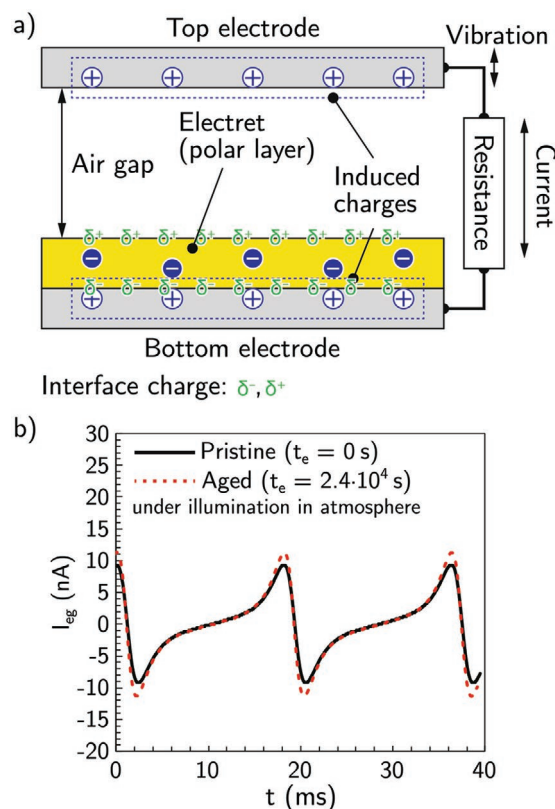


**Figure 12.** Energy harvesting with organic electrets. a) Sketch of a prototype power generator utilizing a polar organic layer as electret. The surface potential difference between top and bottom electrode, introduced by the GSP in the polar layer, generates a current shown in (b), when the distance of the air-gap is periodically changed. (Adapted under the terms of the CC-BY 4.0 license.<sup>[140]</sup> Copyright 2020, The Authors, published by Springer Nature).

states. Thus, we may be forced to make trade-offs between different optimizations of alignment parameters. This in turn requires a sound understanding of the driving forces behind alignment that will allow us to control it. With respect to the frequently used multi-layer device stacks, we therefore need to consider not only the electronic properties of a material that is to be used in a specific function within the device, but also how the layer is processed by controlling substrate temperature or deposition rates during physical vapor deposition. Finally, we may even see some unexpected new applications which exclusively rely on molecular orientation.

## Acknowledgements

This work was funded by the EU Horizon 2020 MSC ITN TADFlife (Grant Agreement No. 812872), by Deutsche Forschungsgemeinschaft (DFG; project Br 1728/20) and by a joint DFG/SNF bilateral funding (Br 1728/22; project no. 432420985).

Open Access funding enabled and organized by Projekt DEAL.

## Conflict of Interest

The authors declare no conflict of interest.

## Keywords

anisotropy, molecular orientation, organic glasses, organic optoelectronics, orientation polarization

Received: May 19, 2021

Revised: July 7, 2021

Published online: August 24, 2021

- [1] S. R. Forrest, *Nature* **2004**, 428, 911.
- [2] S. Reineke, *Nat. Mater.* **2015**, 14, 459.
- [3] M. Schwoerer, H. C. Wolf, *Organic Molecular Solids*, Wiley-VCH, Weinheim, Germany **2006**.
- [4] C. Wöll, *Physical and Chemical Aspects of Organic Electronics: From Fundamentals to Functioning Devices*, Wiley-VCH, Weinheim, Germany **2009**.
- [5] J.-S. Kim, P. K. H. Ho, N. C. Greenham, R. H. Friend, *J. Appl. Phys.* **2000**, 88, 1073.
- [6] K. Hinrichs, M. Levichkova, D. Wynands, K. Walzer, K. J. Eichhorn, P. Bäuerle, K. Leo, M. Riede, *Thin Solid Films* **2012**, 525, 97.
- [7] D. Yokoyama, Z. Q. Wang, Y.-J. Pu, K. Kobayashi, J. Kido, Z. Hong, *Sol. Energy Mater. Sol. Cells* **2012**, 98, 472.
- [8] M. Pope, C. E. Swenberg, *Electronic Processes in Organic Crystals and Polymers*, Oxford University Press, Oxford **1999**.
- [9] N. Karl, *Mol. Cryst. Liq. Cryst. Incorporating Nonlinear Opt.* **1989**, 171, 157.
- [10] D. Yokoyama, *J. Mater. Chem.* **2011**, 21, 19187.
- [11] T. D. Schmidt, T. Lampe, D. Sylvinson M. R., P. I. Djurovich, M. E. Thompson, W. Brütting, *Phys. Rev. Appl.* **2017**, 8, 037001.
- [12] K. Bagchi, M. D. Ediger, *J. Phys. Chem. Lett.* **2020**, 11, 6935.
- [13] F. Schreiber, *Phys. Status Solidi A* **2004**, 201, 1037.
- [14] H. Sirringhaus, P. J. Brown, R. H. Friend, M. M. Nielsen, K. Bechgaard, B. M. W. Langeveld-Voss, A. J. H. Spiering, R. A. J. Janssen, E. W. Meijer, P. Herwig, D. M. de Leeuw, *Nature* **1999**, 401, 685.
- [15] M. Jandke, P. Stroehriegel, J. Gmeiner, W. Brütting, M. Schwoerer, *Adv. Mater.* **1999**, 11, 1518.
- [16] Y.-Y. Lin, D. Gundlach, S. Nelson, T. Jackson, *IEEE Trans. Electron Devices* **1997**, 44, 1325.
- [17] T. Jackson, Y.-Y. Lin, D. Gundlach, H. Klauk, *IEEE J. Sel. Top. Quantum Electron.* **1998**, 4, 100.
- [18] A. C. Dürr, F. Schreiber, M. Münch, N. Karl, B. Krause, V. Kruppa, H. Dosch, *Appl. Phys. Lett.* **2002**, 81, 2276.
- [19] S. Duhm, G. Heimel, I. Salzmann, H. Glowatzki, R. L. Johnson, A. Vollmer, J. P. Rabe, N. Koch, *Nat. Mater.* **2008**, 7, 326.
- [20] Y. Yi, V. Coropceanu, J.-L. Brédas, *J. Am. Chem. Soc.* **2009**, 131, 15777.
- [21] B. P. Rand, D. Cheyns, K. Vasseur, N. C. Giebink, S. Mothy, Y. Yi, V. Coropceanu, D. Beljonne, J. Cornil, J.-L. Brédas, J. Genoe, *Adv. Funct. Mater.* **2012**, 22, 2987.
- [22] U. Hörmann, C. Lorch, A. Hinderhofer, A. Gerlach, M. Gruber, J. Kraus, B. Sykora, S. Grob, T. Linderl, A. Wilke, A. Opitz, R. Hansson, A. S. Anselmo, Y. Ozawa, Y. Nakayama, H. Ishii, N. Koch, E. Moons, F. Schreiber, W. Brütting, *J. Phys. Chem. C* **2014**, 118, 26462.
- [23] V. Vohra, K. Kawashima, T. Kakara, T. Koganezawa, I. Osaka, K. Takimiya, H. Murata, *Nat. Photonics* **2015**, 9, 403.
- [24] J. R. Tumbleston, B. A. Collins, L. Yang, A. C. Stuart, E. Gann, W. Ma, W. You, H. Ade, *Nat. Photonics* **2014**, 8, 385.
- [25] V. Belova, P. Beyer, E. Meister, T. Linderl, M. U. Halbach, M. Gerhard, S. Schmidt, T. Zechel, T. Meisel, A. V. Generalov, A. S. Anselmo, R. Scholz, O. Konovalov, A. Gerlach, M. Koch, A. Hinderhofer, A. Opitz, W. Brütting, F. Schreiber, *J. Am. Chem. Soc.* **2017**, 139, 8474.
- [26] B. Lüssem, M. Riede, K. Leo, *Phys. Status Solidi A* **2013**, 210, 9.
- [27] K. Vandewal, *Annu. Rev. Phys. Chem.* **2016**, 67, 113.
- [28] C. P. Theurer, A. M. Valencia, J. Hausch, C. Zeiser, V. Sivanesan, C. Cocchi, P. Tegeder, K. Broch, *J. Phys. Chem. C* **2021**, 125, 6313.
- [29] M. D. Ediger, J. De Pablo, L. Yu, *Acc. Chem. Res.* **2019**, 52, 407.
- [30] Y. Noguchi, W. Brütting, H. Ishii, *Jpn. J. Appl. Phys.* **2019**, 58, SF0801.
- [31] X. de Vries, R. Coehoorn, *Phys. Rev. Mater.* **2020**, 4, 085602.
- [32] S. Kowarik, A. Gerlach, S. Sellner, F. Schreiber, L. Cavalcanti, O. Konovalov, *Phys. Rev. Lett.* **2006**, 96, 125504.
- [33] L. Penninck, P. de Visschere, J. Beeckman, K. Neyts, *Opt. Express* **2011**, 19, 18558.
- [34] M. K. Callens, D. Yokoyama, K. Neyts, *Opt. Express* **2015**, 23, 21128.
- [35] M. Schmid, T. Morgenstern, W. Brütting, *Org. Electron.* **2018**, 62, 216.
- [36] W. Brütting, J. Frischeisen, T. D. Schmidt, B. J. Scholz, C. Mayr, *Phys. Status Solidi A* **2013**, 210, 44.
- [37] M. Furno, R. Meerheim, S. Hofmann, B. Lüssem, K. Leo, *Phys. Rev. B* **2012**, 85, 115205.
- [38] K. Stavrou, L. G. Franca, A. P. Monkman, *ACS Appl. Electron. Mater.* **2020**, 2, 2868.
- [39] R. Dhali, D. K. A. Phan Huu, F. Bertocchi, C. Sissa, F. Terenziani, A. Painelli, *Phys. Chem. Chem. Phys.* **2021**, 23, 378.
- [40] S. Berleb, W. Brütting, G. Paasch, *Org. Electron.* **2000**, 1, 41.
- [41] E. Ito, Y. Washizu, N. Hayashi, H. Ishii, N. Matsuie, K. Tsuboi, Y. Ouchi, Y. Harima, K. Yamashita, K. Seki, *J. Appl. Phys.* **2002**, 92, 7306.
- [42] K. Bagchi, N. E. Jackson, A. Gujral, C. Huang, M. F. Toney, L. Yu, J. J. de Pablo, M. D. Ediger, *J. Phys. Chem. Lett.* **2019**, 10, 164.
- [43] T. Manaka, K. Yoshizaki, M. Iwamoto, *Curr. Appl. Phys.* **2006**, 6, 877.
- [44] K. Suzuki, S. Kubo, F. Aussenac, F. Engelke, T. Fukushima, H. Kaji, *Angew. Chem., Int. Ed.* **2017**, 56, 14842.
- [45] W. Brütting, S. Berleb, A. G. Mückl, *Org. Electron.* **2001**, 2, 1.
- [46] Y. Noguchi, Y. Miyazaki, Y. Tanaka, N. Sato, Y. Nakayama, T. D. Schmidt, W. Brütting, H. Ishii, *J. Appl. Phys.* **2012**, 111, 11.
- [47] J. Frischeisen, D. Yokoyama, C. Adachi, W. Brütting, *Appl. Phys. Lett.* **2010**, 96, 073302.
- [48] M. Flämmich, M. C. Gather, N. Danz, D. Michaelis, A. H. Bräuer, K. Meerholz, A. Tünnermann, *Org. Electron.* **2010**, 11, 1039.
- [49] J. A. Woollam, B. D. Johs, C. M. Herzinger, J. N. Hilfiker, R. A. Synowicki, C. L. Bungay, in *Optical Metrology: A Critical Review*, Proc. SPIE, Vol. 10294, SPIE, Bellingham, WA **2017**, p. 1029402.
- [50] A. Gujral, K. A. O'Hara, M. F. Toney, M. L. Chabiny, M. D. Ediger, *Chem. Mater.* **2015**, 27, 3341.
- [51] T. Morgenstern, M. Schmid, A. Hofmann, M. Bierling, L. Jäger, W. Brütting, *ACS Appl. Mater. Interfaces* **2018**, 10, 31541.
- [52] M. Flämmich, D. Michaelis, N. Danz, *Org. Electron.* **2011**, 12, 83.
- [53] W. L. Barnes, *J. Mod. Opt.* **1998**, 45, 661.
- [54] M. Flämmich, J. Frischeisen, D. S. Setz, D. Michaelis, B. C. Krummacher, T. D. Schmidt, W. Brütting, N. Danz, *Org. Electron.* **2011**, 12, 1663.
- [55] M. C. Gather, M. Flämmich, N. Danz, D. Michaelis, K. Meerholz, *Appl. Phys. Lett.* **2009**, 94, 263301.
- [56] S. L. M. van Mensfoort, M. Carvelli, M. Megens, D. Wehenkel, M. Bartyzel, H. Greiner, R. A. J. Janssen, R. Coehoorn, *Nat. Photonics* **2010**, 4, 329.
- [57] M. J. Jurov, T. Morgenstern, C. Eisler, J. Kang, E. Penzo, M. Do, M. Engelmayer, W. T. Osowiecki, Y. Bekenstein, C. Tassone, L.-W. Wang, A. P. Alivisatos, W. Brütting, Y. Liu, *Nano Lett.* **2019**, 19, 2489.
- [58] J. Kim, H. Zhao, S. Hou, M. Khatoniar, V. Menon, S. R. Forrest, *Phys. Rev. Appl.* **2020**, 14, 034048.
- [59] H. Ishii, N. Hayashi, E. Ito, Y. Washizu, K. Sugi, Y. Kimura, M. Niwano, Y. Ouchi, K. Seki, *Phys. Status Solidi A* **2004**, 201, 1075.



- [60] Y. Noguchi, H. Lim, T. Isoshima, E. Ito, M. Hara, W. Won Chin, J. Wook Han, H. Kinjo, Y. Ozawa, Y. Nakayama, H. Ishii, *Appl. Phys. Lett.* **2013**, 102, 20.
- [61] K. Osada, K. Goushi, H. Kaji, C. Adachi, H. Ishii, Y. Noguchi, *Org. Electron.* **2018**, 58, 313.
- [62] M. Schmid, K. Harms, C. Degitz, T. Morgenstern, A. Hofmann, P. Friederich, H.-h. Johannes, W. Wenzel, W. Kowalsky, W. Brütting, *ACS Appl. Mater. Interfaces* **2020**, 12, 51709.
- [63] C. Cobet, in, *Ellipsometry of Functional Organic Surfaces and Films* (Eds: K. Hinrichs, K.-J. Eichhorn), Springer Series in Surface Sciences, Vol. 52, Springer, Berlin **2014**, pp. 1–26.
- [64] D. Yokoyama, A. Sakaguchi, M. Suzuki, C. Adachi, *Appl. Phys. Lett.* **2008**, 93, 173302.
- [65] S. S. Dalal, A. Sepúlveda, G. K. Pribil, Z. Fakhraai, M. D. Ediger, *J. Chem. Phys.* **2012**, 136, 204501.
- [66] S. S. Dalal, Z. Fakhraai, M. D. Ediger, *J. Phys. Chem. B* **2013**, 117, 15415.
- [67] G. E. Jellison, F. A. Modine, *Appl. Phys. Lett.* **1996**, 69, 371.
- [68] D. Yokoyama, A. Sakaguchi, M. Suzuki, C. Adachi, *Org. Electron.* **2009**, 10, 127.
- [69] H. G. Tompkins, E. A. Irene, *Handbook of Ellipsometry*, William Andrew Pub and Springer, Norwich, NY and Heidelberg, Germany **2005**.
- [70] R. A. DeCrescent, S. J. Brown, R. A. Schlitz, M. L. Chabiny, J. A. Schuller, *Opt. Express* **2016**, 24, 28842.
- [71] M. Rérat, P. D'Arco, V. Lacivita, F. Pascale, R. Dovesi, *Rend. Lincei, Sci. Fis. Nat.* **2020**, 31, 835.
- [72] W. Kuhn, F. Grün, *Kolloid-Z.* **1942**, 101, 248.
- [73] H. de Vries, *Colloid Polym. Sci.* **1979**, 257, 226.
- [74] A. Hexemer, P. Müller-Buschbaum, *IUCr* **2015**, 2, 106.
- [75] P. Friederich, R. Coehoorn, W. Wenzel, *Chem. Mater.* **2017**, 29, 9528.
- [76] Schrödinger Release 2019-4: Jaguar, Schrödinger, LLC, New York, NY, www.schrodinger.com 2019.
- [77] A. D. Bochevarov, E. Harder, T. F. Hughes, J. R. Greenwood, D. A. Braden, D. M. Philipp, D. Rinaldo, M. D. Halls, J. Zhang, R. A. Friesner, *Int. J. Quantum Chem.* **2013**, 113, 2110.
- [78] V. Rühle, A. Lukyanov, F. May, M. Schrader, T. Vehoff, J. Kirkpatrick, B. Baumeier, D. Andrienko, *J. Chem. Theory Comput.* **2011**, 7, 3335.
- [79] É. Brémond, M. Savarese, N. Q. Su, Á. J. Pérez-Jiménez, X. Xu, J. C. Sancho-García, C. Adamo, *J. Chem. Theory Comput.* **2016**, 12, 459.
- [80] E. Brémond, M. Savarese, C. Adamo, D. Jacquemin, *J. Chem. Theory Comput.* **2018**, 14, 3715.
- [81] C. M. Marian, *Wiley Interdiscip. Rev.: Comput. Mol. Sci.* **2012**, 2, 187.
- [82] W. Koch, M. C. Holthausen, *A Chemist's Guide to Density Functional Theory*, 2nd ed., Wiley-VCH, Weinheim, **2008**.
- [83] D. Jacquemin, C. Adamo, *Int. J. Quantum Chem.* **2012**, 112, 2135.
- [84] C. Adamo, D. Jacquemin, *Chem. Soc. Rev.* **2013**, 42, 845.
- [85] S. Emelyanova, V. Chashchikhin, A. Bagaturyants, *Chem. Phys. Lett.* **2013**, 590, 101.
- [86] B. A. Naqvi, M. Schmid, E. Crovini, P. Sahay, T. Naujoks, F. Rodella, Z. Zhang, P. Stroehriegel, S. Bräse, E. Zysman-Colman, W. Brütting, *Front. Chem.* **2020**, 8, 750.
- [87] C. S. Oh, C.-K. Moon, J. M. Choi, J.-S. Huh, J.-J. Kim, J. Y. Lee, *Org. Electron.* **2017**, 42, 337.
- [88] J. S. Kim, D. Jeong, H. J. Bae, Y. Jung, S. Nam, J. W. Kim, S.-G. Ihn, J. Kim, W.-J. Son, H. Choi, S. Kim, *Adv. Opt. Mater.* **2020**, 8, 2001103.
- [89] P. Friederich, V. Rodin, F. Von Wrochem, W. Wenzel, *ACS Appl. Mater. Interfaces* **2018**, 10, 1881.
- [90] K. Mori, T. P. M. Goumans, E. van Lenthe, F. Wang, *Phys. Chem. Chem. Phys.* **2014**, 16, 14523.
- [91] T. J. Penfold, F. Dias, A. P. Monkman, *Chem. Commun.* **2018**, 54, 3926.
- [92] Y. Wada, H. Nakagawa, S. Matsumoto, Y. Wakisaka, H. Kaji, *Nat. Photonics* **2020**, 14, 643.
- [93] P. J. Hay, *J. Phys. Chem. A* **2002**, 106, 1634.
- [94] K.-H. Kim, E. S. Ahn, J.-S. Huh, Y.-H. Kim, J.-J. Kim, *Chem. Mater.* **2016**, 28, 7505.
- [95] A. Pershin, D. Hall, V. Lemaire, J.-C. Sancho-Garcia, L. Muccioli, E. Zysman-Colman, D. Beljonne, Y. Olivier, *Nat. Commun.* **2019**, 10, 597.
- [96] P. Friederich, F. Symalla, V. Meded, T. Neumann, W. Wenzel, *J. Chem. Theory Comput.* **2014**, 10, 3720.
- [97] T. Northey, J. Stacey, T. J. Penfold, *J. Mater. Chem. C* **2017**, 5, 11001.
- [98] S. Weissenseel, N. A. Drigo, L. G. Kudriashova, M. Schmid, T. Morgenstern, K.-H. Lin, A. Prlj, C. Corminboeuf, A. Sperlich, W. Brütting, M. K. Nazeeruddin, V. Dyakonov, *J. Phys. Chem. C* **2019**, 123, 27778.
- [99] E. Harder, W. Damm, J. Maple, C. Wu, M. Reboul, J. Y. Xiang, L. Wang, D. Lupyan, M. K. Dahlgren, J. L. Knight, J. W. Kaus, D. S. Cerutti, G. Krilov, W. L. Jorgensen, R. Abel, R. A. Friesner, *J. Chem. Theory Comput.* **2016**, 12, 281.
- [100] I. Lyubimov, L. Antony, D. M. Walters, D. Rodney, M. D. Ediger, J. J. de Pablo, *J. Chem. Phys.* **2015**, 143, 094502.
- [101] T. Neumann, D. Danilov, C. Lennartz, W. Wenzel, *J. Comput. Chem.* **2013**, 34, 2716.
- [102] P. Friederich, V. Meded, F. Symalla, M. Elstner, W. Wenzel, *J. Chem. Theory Comput.* **2015**, 11, 560.
- [103] C.-K. Moon, K.-H. Kim, J.-J. Kim, *Nat. Commun.* **2017**, 8, 685.
- [104] Y. Youn, D. Yoo, H. Song, Y. Kang, K. Y. Kim, S. H. Jeon, Y. Cho, K. Chae, S. Han, *J. Mater. Chem. C* **2018**, 75, 4.
- [105] A. Fuchs, T. Steinbrecher, M. S. Mommer, Y. Nagata, M. Elstner, C. Lennartz, *Phys. Chem. Chem. Phys.* **2012**, 14, 4259.
- [106] S. S. Dalal, D. M. Walters, I. Lyubimov, J. J. de Pablo, M. D. Ediger, *Proc. Natl. Acad. Sci. USA* **2015**, 112, 4227.
- [107] M. D. Ediger, *J. Chem. Phys.* **2017**, 147, 210901.
- [108] S. S. Dalal, M. D. Ediger, *J. Phys. Chem. B* **2015**, 119, 3875.
- [109] C. Bishop, A. Gujral, M. F. Toney, L. Yu, M. D. Ediger, *J. Phys. Chem. Lett.* **2019**, 10, 3536.
- [110] C. Mayr, W. Brütting, *Chem. Mater.* **2015**, 27, 2759.
- [111] J. Jiang, D. M. Walters, D. Zhou, M. D. Ediger, *Soft Matter* **2016**, 12, 3265.
- [112] T. Lampe, T. D. Schmidt, M. J. Jurow, P. I. Djurovich, M. E. Thompson, W. Brütting, *Chem. Mater.* **2016**, 28, 712.
- [113] L. Jäger, T. D. Schmidt, W. Brütting, *AIP Adv.* **2016**, 6, 095220.
- [114] H. D. C. N. Gunawardana, K. Osada, K. R. Koswattage, Y. Noguchi, *Surf. Interface Anal.* **2021**, 53, 460.
- [115] K. Sugi, H. Ishii, Y. Kimura, M. Niwano, E. Ito, Y. Washizu, N. Hayashi, Y. Ouchi, K. Seki, *Thin Solid Films* **2004**, 464-465, 412.
- [116] K.-H. Kim, J.-Y. Ma, C.-K. Moon, J.-H. Lee, J. Y. Baek, Y.-H. Kim, J.-J. Kim, *Adv. Opt. Mater.* **2015**, 3, 1191.
- [117] M. J. Jurow, C. Mayr, T. D. Schmidt, T. Lampe, P. I. Djurovich, W. Brütting, M. E. Thompson, *Nat. Mater.* **2016**, 15, 85.
- [118] K.-H. Kim, J.-J. Kim, *Adv. Mater.* **2018**, 30, 1705600.
- [119] K.-H. Kim, J.-L. Liao, S. W. Lee, B. Sim, C.-K. Moon, G.-H. Lee, H. J. Kim, Y. Chi, J.-J. Kim, *Adv. Mater.* **2016**, 28, 2526.
- [120] M. Y. Wong, E. Zysman-Colman, *Adv. Mater.* **2017**, 29, 1605444.
- [121] T. Komino, Y. Sagara, H. Tanaka, Y. Oki, N. Nakamura, H. Fujimoto, C. Adachi, *Appl. Phys. Lett.* **2016**, 108, 24.
- [122] Y. Watanabe, D. Yokoyama, T. Koganezawa, H. Katagiri, T. Ito, S. Ohisa, T. Chiba, H. Sasabe, J. Kido, *Adv. Mater.* **2019**, 31, 1808300.
- [123] R. A. Marcus, *J. Chem. Phys.* **1956**, 24, 966.
- [124] D. Yokoyama, Y. Setoguchi, A. Sakaguchi, M. Suzuki, C. Adachi, *Adv. Funct. Mater.* **2010**, 20, 386.
- [125] H. Ishii, K. Sugiyama, E. Ito, K. Seki, *Adv. Mater.* **1999**, 11, 605.
- [126] I. H. Campbell, S. Rubin, T. A. Zawodzinski, J. D. Kress, R. L. Martin, D. L. Smith, N. N. Barashkov, J. P. Ferraris, *Phys. Rev. B* **1996**, 54, R14321.
- [127] H. Kinjo, H. Lim, T. Sato, Y. Noguchi, Y. Nakayama, H. Ishii, *Appl. Phys. Express* **2016**, 9, 021601.

- [128] S. Altazin, S. Züfle, E. Knapp, C. Kirsch, T. Schmidt, L. Jäger, Y. Noguchi, W. Brütting, B. Ruhstaller, *Org. Electron.* **2016**, 39, 244.
- [129] A. J. L. Hofmann, S. Züfle, K. Shimizu, M. Schmid, V. Wessels, L. Jäger, S. Altazin, K. Ikegami, M. R. Khan, D. Neher, H. Ishii, B. Ruhstaller, W. Brütting, *Phys. Rev. Appl.* **2019**, 12, 064052.
- [130] S.-Y. Kim, W.-I. Jeong, C. Mayr, Y.-S. Park, K.-H. Kim, J.-H. Lee, C.-K. Moon, W. Brütting, J.-J. Kim, *Adv. Funct. Mater.* **2013**, 23, 3896.
- [131] J. Frischeisen, D. Yokoyama, A. Endo, C. Adachi, W. Brütting, *Org. Electron.* **2011**, 12, 809.
- [132] Y.-S. Tyan, *J. Photonics Energy* **2011**, 1, 011009.
- [133] M. C. Gather, S. Reineke, *J. Photonics Energy* **2015**, 5, 057607.
- [134] T. D. Schmidt, D. S. Setz, M. Flämmich, J. Frischeisen, D. Michaelis, C. Mayr, A. F. Rausch, T. Wehlus, B. J. Scholz, T. C. G. Reusch, N. Danz, W. Brütting, *Appl. Phys. Lett.* **2013**, 103, 093303.
- [135] Y. Esaki, T. Komino, T. Matsushima, C. Adachi, *J. Phys. Chem. Lett.* **2017**, 8, 5891.
- [136] J. Ràfols-Ribé, P.-A. Will, C. Hänisch, M. Gonzalez-Silveira, S. Lenk, J. Rodríguez-Viejo, S. Reineke, *Sci. Adv.* **2018**, 4, eaar8332.
- [137] J. S. Bangsund, J. R. Van Sambeek, N. M. Concannon, R. J. Holmes, *Sci. Adv.* **2020**, 6, eabb2659.
- [138] T. Ferschke, A. Hofmann, W. Brütting, J. Pflaum, *ACS Appl. Electron. Mater.* **2020**, 2, 186.
- [139] Y. Ueda, H. Nakanotani, T. Hosokai, Y. Tanaka, H. Hamada, H. Ishii, S. Santo, C. Adachi, *Adv. Opt. Mater.* **2020**, 8, 2000896.
- [140] Y. Tanaka, N. Matsuura, H. Ishii, *Sci. Rep.* **2020**, 10, 6648.



**Alexander Hofmann** studied physics at the University of Augsburg and finished his master thesis on organic solar cells in 2014. He later switched subject to organic light emitting diodes and received his Ph.D. degree in physics in 2020, studying the influence of oriented polar organic material on the electric properties of OLEDs. His current research topics focus on the manifold effects of optical and electrical alignment of organic optoelectronics, in both OLED and OPV.



**Markus Schmid** received his M.Sc. from the Institute of Physics at the University of Augsburg in 2017. During his master thesis, he already worked in the research group of professor Brütting and joined the team as a Ph.D. candidate, after that. The focus of his research lies on identifying the basic mechanisms that lead to a preferential orientation in small molecule organic thin films. His studies cover different classes of materials, like phosphorescent iridium complexes as well as fluorescent dyes and neat host materials.



**Wolfgang Brütting** received his Ph.D. in Physics from the University of Bayreuth in 1995 with a work on charge-density wave systems. Thereafter he moved to the field of organic semi-conductors where he could take part in the development of organic light-emitting diodes for display applications. In 2003 he became professor for Experimental Physics at the University of Augsburg. His current research activities include charge transport and photophysics of organic semi-conductors and their device physics. He has published more than 200 journal articles, several book chapters and edited the book *Physics of Organic Semiconductors*.